GeoScienceWorld
Lithosphere
Volume 2022, Article ID 2632112, 19 pages
https://doi.org/10.2113/2022/2632112

Lithosphere

Research Article

A Dramatic Marine Environment Change in the Beibu Gulf of the South China Sea around 3.2 kyr BP

Zhou Guoyi,[1,2,3] **Cao Xinxing**,[4] **Xia Jia**,[5] **Wang Sibo**,[5] **and Song Zhiguang**[1,2]

[1]*State Key Laboratory of Organic Geochemistry, Guangzhou Institute of Geochemistry, Chinese Academy of Sciences, Guangzhou 510640, China*
[2]*CAS Center for Excellence in Deep Earth Science, Guangzhou 510640, China*
[3]*The University of Chinese Academy of Sciences, Beijing 100049, China*
[4]*Key Laboratory of Beibu Gulf Environmental Change and Resources Utilization of Ministry of Education, Nanning Normal University, Nanning 530001, China*
[5]*College of Chemistry and Environmental Science, Guangdong Ocean University, Zhanjiang 524088, China*

Correspondence should be addressed to Song Zhiguang; zsong@gig.ac.cn

Received 31 December 2021; Accepted 12 May 2022; Published 18 June 2022

Academic Editor: Shengfa Liu

The profile geochemical characteristics of a seafloor sediment core, collected from the Beibu Gulf of the South China Sea, have been investigated in terms of the sediment grain size, the content of major and trace elements, the total organic carbon (TOC) and organic nitrogen (TN), and the carbon isotopic composition of organic matter ($\delta^{13}C_{org}$) and AMS ^{14}C dating. These results show that the core sediments were deposited since 11.3 kyr BP and the profile could be clearly divided into the lower and upper sediment section based on geochemical characteristics. The lower section covers the depth of 86 cm to 200 cm and was deposited from 3.2 to 11.3 kyr BP, while the upper section is at the depth of 4 to 86 cm and represents sediments from 0.2 to 3.2 kyr BP. The upper section sediments are charcteristized by a much finer grain size and a clearly positive deviation of the $\delta^{13}C_{org}$ value. Obviously, the overall profile geochemical characteristics indicate that the upper section was deposited under a significantly deeper seawater depth associated with a relatively weaker hydrodynamic and a better preservation condition for organic matter, while the low section was deposited under a relatively shallow seawater depth with the relatively stronger hydrodynamic condition and a relatively poor preservation condition for organic matter. Finally, it is suggested that the transition between the lower section and the upper section occurring around 3.2 kyr BP was mostly likely due to a dramatic marine environmental change caused by the rapid seafloor subsidence associated with the further expansion of the Qiongzhou Strait. And further multidisciplinary studies are needed to better reveal and understand different aspects of the significance of this marine environment change in the Beibu Gulf of the South China Sea.

1. Introduction

The South China Sea (SCS) is the largest marginal sea on the western side of the Pacific Ocean, and its marine environment has a great impact on the continental climate environment of China [1]. Therefore, the study on its marine environment changes is of great significance for understanding and predicting the regional climatic variation in East Asia in the future [2]. Marine sediments in the coastal continental shelf are supposed to preserve the geochemical information of marine environmental change related to the regional and global climates. Many studies had been carried out on the geochemical characteristics of marine sediments in the northern region of the South China Sea. And these studies have provided significant information on the fluctuation of sea level, the intrusion of the Kuroshio invasion, the intensity of solar insolation, the input changes in sedimentary sources, and the weathering condition and erosion process in the surrounding continents [3–8]. However, most of these previous studies focused on the coastal area of the Pearl River

Estuary in eastern Guangdong province, China [9–12]. Few studies have been carried out on the marine environmental changes in the Beibu Gulf region of the South China Sea.

The Beibu Gulf is located in the northwest continental shelf area of the South China Sea, which is a semiclosed bay surrounded by land on three sides and mainly affected by the diurnal tide. With the specific geographical location, diversified submarine topography and the complex of sea surface currents and hydrodynamic environments, the marine environment changes of the Beibu Gulf would significantly influence the regional climate condition, especially the South China region and surrounding continents. Several studies had been carried on the Holocene sediments from the Beibu Gulf of the South China Sea concerning the regional climate and marine environment changes. The Holocene marine sediments in the Beibu Gulf area are mainly clay silt or silt that were mainly deposited since 10.8 kyr BP. Due to the primary differences in the arrival time of Holocene transgression reaching to the coastal area of the Beibu Gulf, hydrodynamic conditions, submarine topography, and supply of sediment, the main Holocene sediment thickness in the Beibu Gulf sea area was about 2-22 m [13–18]. Some studies have been carried out on the geochemical characteristics of the Holocene marine sediments and reefs from the coastal areas of Guangxi Province and Vietnam's Red River delta in the northern region of the Beibu Gulf to understand the regional environmental changes, sea level changes, and marine transgression [18–23]. Furthermore, the growth and extinction of coral reefs offshore the Leizhou peninsula have also been studied to reconstruct the sea surface temperature (SST) variation [24–26].

The Holocene, starting at the end of the colder Younger Dryas cooling episode around 11.7 kyr BP, is a warmer climate period accompanied by several cold fluctuations that are intermitted for 8 to 10 times on decade to century-scale [27]. These Holocene cold fluctuations were mainly related to solar insolation and atmospheric circulation changes [28], such as 8.2 kyr BP, 4.2 kyr BP, and the Little Ice Age cold events, and they were usually superimposed on the millennial-scale cold events with the slow cooling trend [29, 30]. It is widely accepted that these low-frequency millennial-scale cold events (Holocene 1500-year-cycle rapid change climate events) in the northern hemisphere were predominantly forced by the decrease of solar insolation induced by the variation of the earth's orbital, the southward shift of the intertropical convergence zone (ITCZ), and the subsequent weakening of the summer monsoon strength [27, 31–33], while the mechanisms of these cold fluctuations are assumed to be closely related to the increase of ice meltwater flux in the North Atlantic in the early Holocene [33], the synergistic effect of the enhancement of volcanic activity and the decrease of sunspot activity in the late Holocene [34, 35], and the fluctuation of thermohaline circulation or the complex interaction between the ocean and atmosphere [36, 37]. In addition, the Holocene is also a significant period in which human activities also increasingly enhanced the transformation of the earth's environment, such as the formation of the ozone hole, soil desertification, acid rain and haze, and the aggravation of the greenhouse effect.

Obviously, the geochemical study of marine sediments is important to understand the regional marine environment change and its effects on the regional climate change in the Beibu Gulf of the South China Sea since the Holocene. Therefore, by investigating the profile variation of sediment grain size (Mz); the content of TOC, TN, and major and trace elements; and the $\delta^{13}C_{org}$ composition in a sediment core collected from the northeastern Beibu Gulf of the South China Sea, this study was aimed at providing high-resolution information on the marine environment changes and possible climate responses in the Beibu Gulf region, as well as deepening the understanding of marine environmental changes in the marginal sea and its correlation to the global climate change since the Holocene.

2. Material and Methods

2.1. Geological and Geographic Background of the Beibu Gulf. Located on the northwest margin of the South China Sea, the Beibu Gulf is a semienclosed bay with an area of about 12.93×10^4 km^2 and lies in the continental shelf sedimentary area [38]. The Beibu Gulf is surrounded by land on three sides and has been developed since the Holocene along with the global sea level rise. In geology tectonics, the Beibu Gulf is considered as an intracontinental rift basin dominated by Cenozoic sedimentation and is mainly distributed by two secondary sedimentary basins, the Beibuwan basin and the Yinggehai basin. And these two basins are largely controlled by a number of NE- and NW-trending faults, respectively (Figure 1). For the land surrounding the Beibu Gulf, the Paleozoic and Mesozoic sedimentary rocks are widely exposed in the west of the Beibu Gulf; Mesozoic and Quaternary sedimentary rocks and Holocene sediments are dominated in the northern coast of the Beibu Gulf; Holocene marine deposits are mainly distributed in the north of the Leizhou Peninsula on the eastern coast of Beibu Gulf; meanwhile, basalt rocks are mainly exposed contemporarily in the south. As for Hainan Island, there are also extensive late Quaternary basalt outcrops in the northern part of Hainan Island, and Quaternary deposits are mainly distributed near the coastal zone (Figure 1).

The Beibu Gulf is connected to the South China Sea through the bay mouth in the south and the Qiongzhou Strait in the east. The water depth in the Beibu Gulf is less than 100 m, and the average water depth is about 40 m. The submarine topography is obviously restricted by the coast, isobath lines arranged along the north shoreline of Beibu Gulf are toward the NE-SW direction, and the southern part is turned to the NW-SE direction (Figure 1). The Beibu Gulf is geographically situated in the tropic and subtropic zone with an annual air temperature varying from -0.8 to 37.4°C (averaged at 22.4°C), and the annual rainfall is above 1700 mm with an average of about 2150 mm [39]. And several rivers flow into the Beibu Gulf, such as the Changhua River in Hainan Island; Jiuzhou River in Guangdong; Nanliu River, Qin River, Maoling River, Fangcheng River, and Beilun River in Guangxi Zhuang

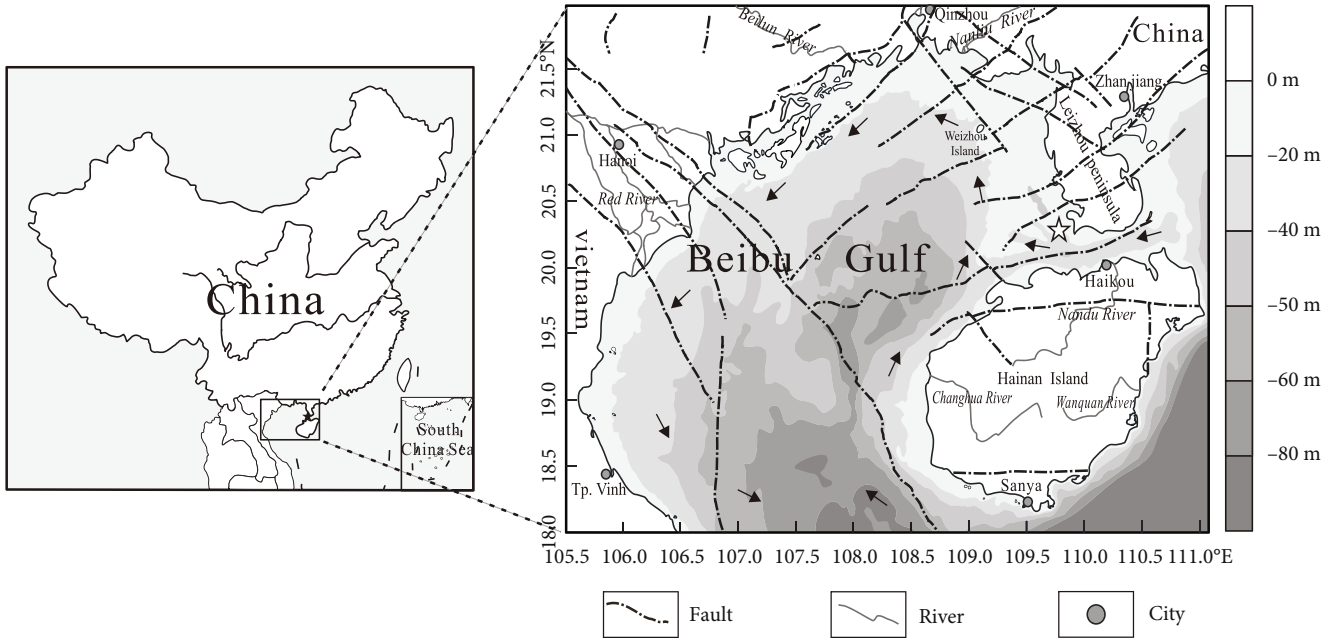

FIGURE 1: Locations of P36 sediment core in the Beibu Gulf (modified after [14, 17, 69]). Note that the dotted lines represent the main faults in the Beibu Gulf, the arrows indicate the main direction of the sea current, and the hollow asterisk represents the location of the P36 core.

Autonomous Region; and the Red River, Taiping River, and Ma Jiang River in Vietnam. Moreover, because the Beibu Gulf is significantly influenced by the East Asian monsoon, its seawater circulation pattern is quite complicated, with the northeastward surface current prevailing in summer but the southwestward surface current dominating in winter. The surface current of the Beibu Gulf displays a distinct counterclockwise cycle pattern in both summer and winter under the common influence of the East Asian monsoon, the tide current of Qiongzhou Strait, and the seawater density gradient and the submarine topography of the Beibu Gulf [40–42].

2.2. Sample Collection. The sediment core was collected using the gravity piston sampler during the comprehensive scientific excursion of offshore marine environment and ecology survey surrounding the Leizhou Peninsula in October of 2017. The core sediments were collected in the sampling site of P36 which is located at the periphery of Dongchang Bay in the southwest offshore area of Leizhou Peninsula (109°50.744′ E, 20°17.902′ N) with a water depth of 15.5 m (Figure 1). The sediment core is about 2 m long with good viscosity. The physical property of core sediments appears to be in a status of uniformly fluid-soft plastic mud. The sediments contain barely any shell debris in the lower part of this core profile, but some kinds of shell debris such as bivalves and gastropod shell residuals are occasionally seen in the upper part of the core profile.

Once the sediment core was taken from the seabed, it was immediately sectioned in the cabin laboratory of the boat. The core samples were sliced into 99 samples at every 2 cm interval except that the top 0-4 cm sediment layer of the profile was discarded to avoid the effect of the benthic bioturbation, resuspension, and seafloor redeposition. All samples were wrapped up using presterilized aluminum foil and sealed into sterile polyethylene bags and then stored in the freezer on the ship. Up to the completion of this scientific excursion, a total of 49 core sediment samples from the core profile were taken for this study in an order of every other 2 cm thick samples, and then, the samples were transported to the laboratory and stored below -20°C until further treatments and analysis.

2.3. AMS ^{14}C Dating of Core Sediments. The core sediments used for ^{14}C dating were first treated using hydrochloric acid to remove the inorganic carbonate, and then, sediment solid residues were heated in the elemental analyzer to convert the organic carbon into CO_2 according to the method of Chen et al. [43]. After the CO_2 gas was purified and converted into graphite during hydrogen reduction with the iron or cobalt catalyst using the ion automatic graphitization equipment, the ^{14}C content of the converted graphite target sample was measured by the accelerator mass spectrometer (NEC 0.5MV 1.5SDH-1AMS) with the 0.3% instrument analytic error. All AMS ^{14}C ages were calibrated into the calendar ages by using the Calib 8.2 calibration program (http://calib.org/calib/calib.html) developed by Minze Stuiver of Quaternary Isotope Laboratory, University of Washington, USA. According to the marine radiocarbon calibration curve (Marine 20) [44], the ^{14}C calendar age of sediments was corrected with the regional ocean carbon reservoir correction value (ΔR) [45] in different periods of the Holocene by using the data of Hua et al. [46].

2.4. Sediment Grain Size Analysis. For sediment grain size analyses, about 0.5 g of sediment samples were packed into

a 10 ml centrifuge tube and excess 10 N hydrogen peroxide solution was added to oxide the organic matter for 12 hours. And then, the solution was treated with 6 N hydrochloric acid for another 12 hours to remove the carbonate portion. After the solid residues were rinsed and centrifuged with deionized water six times, they were saturated with 0.5% solution of sodium hexametaphosphate ($(NaPO_3)_6$) as the dispersant for 24 hours. Finally, the sediment residues with saturated dispersant were subjected to grain size analyses by using the Malvern MasterSizer 2000 laser particle size analyzer. The measurement size range of this instrument is 0.02-2000 μm, the resolution is above 0.01Φ, and the repeating relative error is less than 1%. The relative content of clay fraction (>4 μm), silt fraction (4-63 μm), and sand fraction (>63 μm) is determined by the cumulative percentage of the grain size distribution [47].

2.5. Bulk Organic Matter Analysis of Core Sediments. The TOC and TN of sediment samples were determined with a Vario EL-III Elemental Analyzer. The dried and homogenized sediment powder samples were first acidified with 10% (v/v) hydrochloric acid for 24 h to remove the inorganic carbon. After the solid residues were rinsed and centrifuged with deionized water for 8 times until them became neutral (pH = 7), the solid residues were then dried at 60°C before the analysis. The parallel sample was measured for each sample, and the standard deviation of replicate analysis of every sample was less than ±0.02 wt% (C) and ±0.005 wt% (N).

The organic carbon isotope analysis of carbonate-free sediment samples was performed by using the Finigan Element Analysis-isotope ratio mass spectrometer (Delta XL Plus EA-IRMS). The residue samples were mixed with the appropriate amount of rod-like copper oxide and platinum wire as the catalyst and burned in an oxidation furnace at 800 to 850°C for 10 min. And the generated CO_2 gas was condensed and purified through a cold trap of liquid nitrogen and then released for the carbon isotope ratio measurement. The reference standard carbon isotopic sample is Vienna Pee Dee Belemnite (PDB). The standard deviation of replicate measurements of samples was less than ±0.04‰ for $\delta^{13}C_{org}$.

2.6. Analysis of Major and Trace Elements. The freeze-dried powder samples of 200 mesh were heated at 110°C for 6 h and then were combusted at 900°C for 3 h to remove organic matter. The residues were mixed with the fluxing agent ($Li_2B_4O_7$) in a weight ratio of 1 : 8 in a Pt-Au crucible, and then, the mixtures were transferred into the melting machine to make fusible glass pieces. Finally, the content of major element oxides was determined using the Rigaku X-ray fluorescence spectrometer (XRF, ZSX 100e). The analytical accuracy for major elements was better than 1%, and the relative standard deviation of measurement is no more than 5%. As for trace elements, about 30-45 mg powder samples were heated at 600°C for 2 h and then digested with a mixture solution of HNO_3+HF in a Pt crucible on an electric hot plate. And the eluted solution was diluted by 2% HNO_3 for trace-element measurements using the Inductively Coupled Plasma Mass Spectrometry (ICP-MS) with a PlasmaQuant mass spectrometer. Analytical precision and accuracy were monitored by repeating analyses of OU-6, AGV-2, and GBPG-1 standards. The relative standard deviation was less than 10%, and the analytical precision was better than 10%.

The chemical index of alteration (CIA) was used to reconstruct dry and wet changes in the provenance of sediments by using the following formula [48]:

$$\mathrm{CIA} = \frac{\mathrm{Al_2O_3}}{\mathrm{Al_2O_3} + \mathrm{CaO^*} + \mathrm{Na_2O} + \mathrm{K_2O}} * 100 \quad (1)$$

Here, CaO^* refers to the Ca content in the silicate fraction of sediments excluding the Ca in minerals such as carbonate and phosphate. Because the CIA was calculated by the ignition loss method, not by adopting the method of acid dissolution to remove the Ca constituent in silicate minerals, we adopted the correction method that Mclennan [49] summarized, namely, according to the following formula: $n(CaO') = n(CaO) - 10 * n(P_2O_5)/3$ to calculate the CIA; if the value of $n(CaO') > n(Na_2O)$, we use the Na_2O molar content instead of the CaO^* content; otherwise, the CaO^* content is calculated directly by the molar content of CaO'.

3. Results

3.1. Age Dating and Deposition Rate of Core Sediments. The AMS ^{14}C dating results of the P36 core sediments are listed in Table 1. Due to the inexplicable reversal of the age data at the burial depth of 196-198 cm, the age of sediment samples below 154 cm is unreliable. On the other hand, because the surface layer of 10 cm of the seafloor sediments in the coastal shelf are often disturbed by the bioturbation, resuspension, and redeposition, the dating age of 790 a BP at the burial depth of 4-6 cm is likely inappropriate. The dating ages of sediments at the depth of 48-50 cm (1700 a BP) to the 152-154 cm sedimentary layer (8740 a BP) were used as the control points, and the Bayesian age-depth model was used to obtain more integrated and accurate age information of the P36 sediment core [50].

According to the Bayesian age-depth model, the age of the bottom of the P36 core was estimated as 11.3 kyr BP (Figure 2(d)). The burial depth of 200 to 86 cm was deposited from 11.3 to 3.2 kyr BP, which coincided with the sea level rise stage during the early-middle Holocene [51, 52] associated with a deposition rate of 14.07 cm/kyr. The upper section of 86 to 4 cm was dated as deposited from 3.2 to 0.2 kyr BP, and there was an accelerated sedimentation process with a higher deposition rate of 27.33 cm/kyr. Although these calculated deposition rates do not consider the compaction factor, the variation in deposition rate, in particular between the upper section and the lower section, suggests that the sedimentary environment has changed, and this change may be related to the basin subsidence, sea level change, or sediment supply.

3.2. Profile Distribution of Sediment Grain Size. The grain size distribution of the sediment is an important indicator

Table 1: AMS ^{14}C dating of core sediment.

Sample name	Depth (cm)	Material	Conventional age (^{14}C yr BP)	2σ cal BP[a]	Probability[b]	Mean (cal yr BP)[c]
TS-1	4-6	Sediment	1840 ± 35	641-954	1.000	790
TS-12	48-50	Sediment	2380 ± 35	1485-1932	1.000	1700
TS-21	84-86	Sediment	3325 ± 40	2671-3117	1.000	2890
TS-29	116-118	Sediment	5025 ± 45	4891-5367	1.000	5150
TS-38	152-154	Sediment	8545 ± 50	8416-9033	1.000	8740
TS-49	196-198	Sediment	4700 ± 35	4853-5278	1.000	5060

Note: [a]relative area under the distribution curve. [b]Precision is 2-sigma in the program Calib 8.20. [c]The intermediate age with the maximum probability rounded to the nearest multiple of 10 yr.

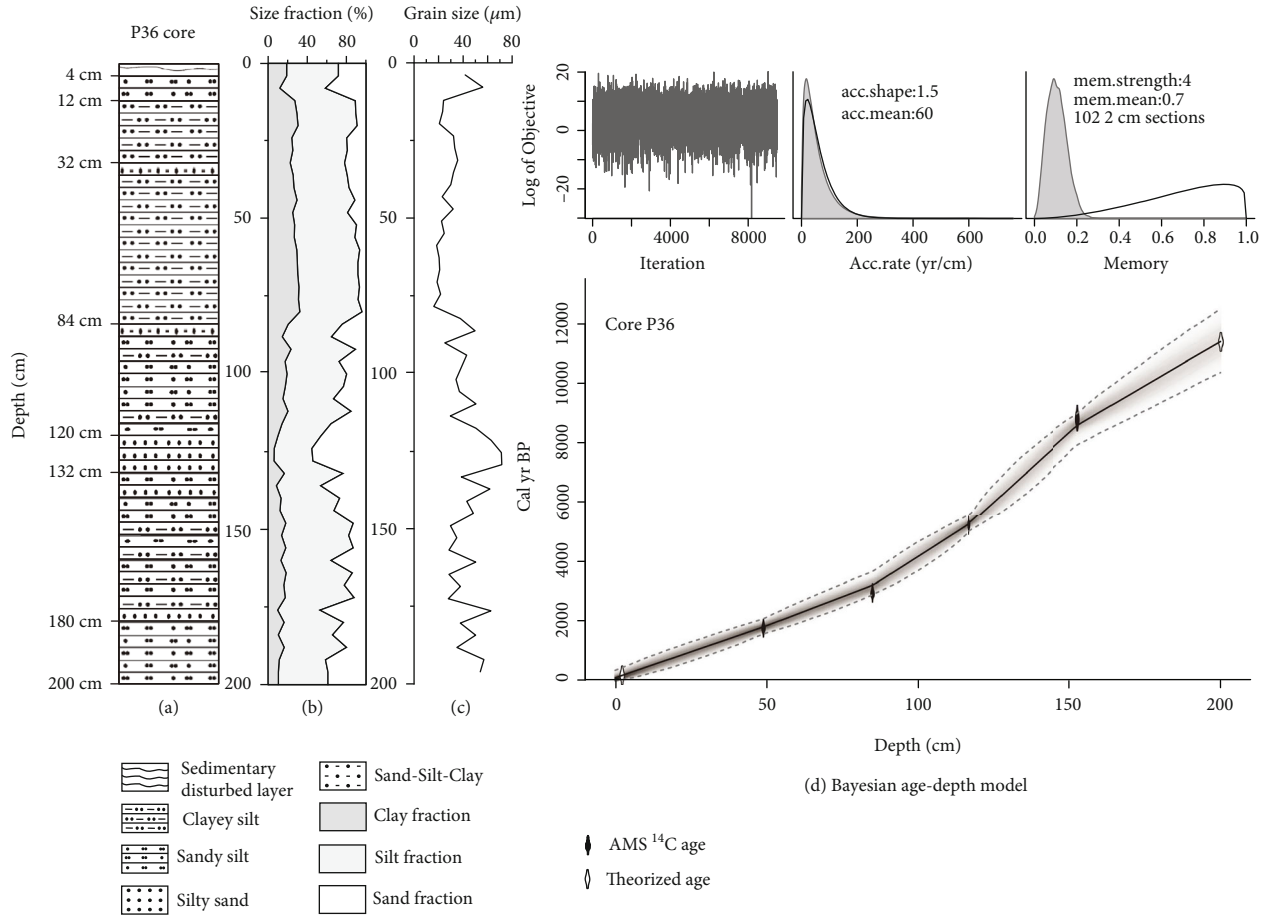

Figure 2: Lithologic characteristics and Bayesian age-depth model of the core P36. Note: (a) lithological column; (b) core sediment size fraction (clay, %; silt, %; and sand, %); (c) the sediment mean grain size (μm); (d) the Bayesian age-depth model of the core P36.

of the sedimentary environment and sedimentary dynamic conditions which is related to the sediment source, transport medium, transport mode, and sedimentary environment. The lithology of the P36 core is mainly composed of clayey silt interbedded with sandy silt, especially for the lower section sediments (Figure 2(a)). As to the profile variation of the sediment grain size fraction, the P36 core sediments are dominated by silt fraction with a content of 38.7% to 70.7% and averaged at 57.5%. However, the sand fraction content, which is much less than that of the silt fraction, varies greatly with an average of 27.9%. And the content of clay is relatively lower ranging from 5.9% to 32.3% with an average of 19.5% (Figure 2(b)).

And the mean grain size of the P36 core ranges from 16.1 μm to 71.6 μm and also displays a clear two-section variation on the profile (Figure 2(c)). Between them, the low section covers the depth of 86 cm to the bottom of the profile and is characterized by a dominant but variable silt fraction associated with relative higher and variable content of sand fraction and lower content of clay fraction (Figure 2(b)).

And the mean grain size of these section sediments varies greatly from 25.1 to 71.6 μm (Figure 2(c)), while the upper section ranges from the depth of 86 cm to 4 cm, and sediments in the upper section are dominated by a higher and more stable content of silt fraction with relatively higher content of fine clay fraction and lower content of sandy fraction (Figure 2(b)). And the mean grain size of sediments is in the range of 16.1 to 56.0 μm but remains steady at around 36 μm for the most part of this section (Figure 2(c)). The clay fraction displays a significant increase in the upper section (11.9 to 32.4%) compared to the lower section (5.9% to 23.3%). Besides, it should be pointed out that there is a clear drop in the clay fraction and a significant increase in the sand fraction at the depth of 12-4 cm in the upper section (Figure 2(b)) which may suggest that there was an another environmental change in the Beibu Gulf and it would be worthwhile to do more studies.

It is interesting to point out that the profile division based on the grain size distribution of the P36 core profile timely coincides with the profile division of the deposition rate based on the age dating. Obviously, it is not a coincidence but indicates that the marine environment has experienced significant change since the 3.2 kyr BP, and this change was remarkably affected by the deposition rate, sediment size distribution, and other sedimentary features. And the grain size distribution also indirectly proves that the dating ages and related deposition rate are reliable for the division of the sediment profiles as the upper deposition rate coincides with the upper section sediments and the lower deposition rate matches the lower section sediments. It is noticeable that a significant change in the sediment grain size distribution and the deposition rate has occurred at the depth of 4 to 86 cm since the dating age of 3.2 kyr BP on the profile, and these suggest that 3.2 kyr BP is a critical period for the marine environment change in the Beibu Gulf.

3.3. The Profile Variation of TOC, TN, C/N Ratio, and $\delta^{13}C_{org}$. The TOC of the P36 core sediments ranges from 0.23% to 0.62%, with an average value of 0.40%, and the TN content is in the range of 0.04% to 0.09%, with an average value of 0.06% (Figure 3). As for the $\delta^{13}C_{org}$ in the core sediments, it varies from 24.14‰ to -21.54‰ with an average of -22.72‰ and indicates that the majority of organic matter (OM) is the marine autogenous source input [53]. The profile variation of these three proxies displays the same pattern as that of grain size distribution and the deposition rate. Therefore, the profile of P36 core sediments could also be divided into the upper and lower sections according to the profile distribution of these three proxies. The lower section is at the depth of 86-200 cm, which is dated as deposited from 11.3 to 3.2 kyr BP, and is characterized by lower TOC and TN contents and the relative negative deviation of $\delta^{13}C_{org}$ composition ranging from 0.23% to 0.40%, 0.04 to 0.06%, and -24.14‰ to -22.45‰, respectively, while the upper section is at the depth of 4-86 cm with the dating age of 3.2 kyr BP to 0.2 kyr BP and is featured by higher values of TOC and TN contents and relative positive $\delta^{13}C_{org}$ composition with the range from 0.38 to 0.62%, 0.06 to 0.09%, and -21.29‰ to -22.09‰, respectively.

The C/N ratio is an important indicator for the source of OM in sediments. Generally, the C/N ratio of marine plankton is between 5 and 7 [54], and terrestrial vascular plants show a value of ≥12 due to being rich in lignin and cellulose [55], while a C/N ratio of 8 to 12 is considered as a mixture of marine and terrigenous sources [56]. The C/N ratio in the P36 core sediments is in a range of 6.4 to 8.2 and this ratio range indicates that the source of sedimentary OM is almost unchanged during the whole deposition of the P36 sediment profile and is mainly the marine autogenous source mixed with a significant proportion of terrigenous input in the Beibu Gulf. Thus, the higher TOC content and relative positive deviation of $\delta^{13}C_{org}$ composition in the upper section sediments significantly indicate that during the upper section deposition period, the marine autogenous OM input was increased compared to that of the lower section with a better preservation condition.

3.4. The Profile Distribution of Major and Trace Elements. The content and profile variation of most major and trace elements also display a similar two-section pattern as that of sediment grain size and OM (Figure 4). The contents of major element Si and Ca and trace element Zr, Sr, and Hf that are mainly enriched in the terrigenous clastic composition including coarser quartz and feldspar are significantly lower in the upper section sediments compared to the lower section sediments (Figure 4), while the contents of A1, Fe, Ti, P, V, Cr, and Mn that tend to be enriched in fine clay fractions are clearly higher in the upper section compared to the lower section sediments (Figure 4), indicating a significant negative correlation relationship with the sediment grain size (Figure 5 and Table 2).

The significant differences in these element contents between the upper and lower sections are largely due to the grain size changes and reflect that the preference enrichment of these elements is associated with different sizes of clastic or clay minerals. Therefore, this profile distribution of elements also indicates the significant change in the sedimentary environment during the deposition of the upper and lower section sediments since the 3.2 kyr BP. On the other hand, the contents of soluble major elements Na, K, Mg, and trace element Ba show no significant variation on the whole profile, and this may suggest that the salinity of seawater had remained unchanged during the whole deposition of the profile.

4. Discussion

4.1. The Profile Variation of Sediment Grain Size Distribution. Sediment grain size can be used to determine the sedimentary environment and the hydrodynamic conditions that are controlled by material source, transport medium, migration pattern, and sedimentary environment. In general, the grain size of P36 core sediments is in the range of 20 to 60 μm, which represents nearshore-suspension and coarse-silt sediments [57–59]. This grain size range indicates that the sedimentary environment in the region of this sediment core was in a relatively strong hydrodynamic condition.

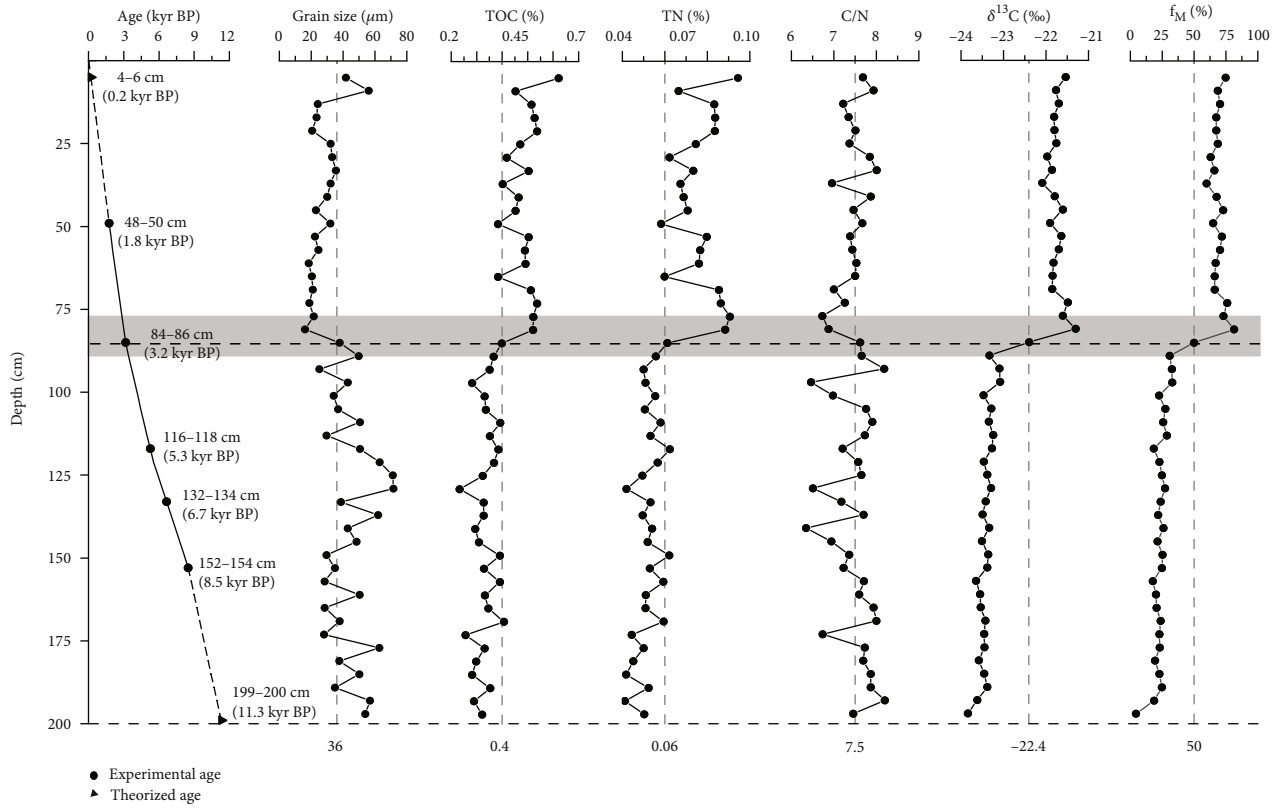

FIGURE 3: Profile changes of core sediment age model, mean grain size distribution, total organic carbon (TOC) content, total organic nitrogen (TN), C/N elemental ratio, the carbon stable isotopic value of organic matter ($\delta^{13}C_{org}$), and the proportion of marine and terrestrial organic carbon in the TOC in the P36 core. Note: the shaded region shows distinct depositional transition (76-90 cm) around the 3.2 kyr BP on the profile.

On the other hand, the grain size distribution between the upper and lower sections clearly suggests that the hydrodynamic condition was a significant difference between the lower and upper section sediments.

The higher proportion of sandy grain and frequent fluctuation of the grain size distribution in the lower section sediments suggest that the lower section sediments were deposited under the relatively stronger hydrodynamic condition associated with the frequent fluctuation of hydrodynamic condition during sedimentation (Figure 3), while the relatively finer grain size and stable size distribution of the upper section sediments indicate that the hydrodynamic condition was relatively weaker but more stable through the sedimentation period compared to those of the lower section (Figure 3). In the marginal seas, the shallow water often corresponds to the stronger hydrodynamic condition while the deeper water usually suggests the weaker hydrodynamic condition. Therefore, the lower section sediments were deposited under the shallow water associated with the stronger but variable hydrodynamic condition. In contrast, the upper section sediments were developed under deeper water associated with the weaker but stable hydrodynamic condition. On the other hand, the hydrodynamic condition changes are often correlated with the water depth or sea level change, so it is certainly true that the seawater depth at the location of the P36 core experienced a long-term change from shallow water to deeper water around 3.2 kyr BP.

4.2. The Source and Contribution of Organic Matter. The higher OM in sediments often results from either a better preservation condition or a higher organic input. The two-section distribution pattern of the TOC content in P36 core sediments suggests that there were differences in the organic matter inputs and preservation conditions between the upper and lower section sediments. The strong linear positive correlation between TOC and TN (Figure 6(f)) also indicates that the TN is mainly organic nitrogen and the source of sedimentary OM was always consistent, rather than the inorganic nitrogen (NH_4^+) being adsorbed and brought by clay minerals to core sediments [60], while a stable TOC/TN ratio (6.4 to 8.2) on the whole P36 core profile (Figure 3) implies that the major source of OM was almost unchanged and was dominated by the marine autogenous source during the sedimentation of the P36 core. Moreover, the $\delta^{13}C_{org}$ in the core sediments also displays a two-stage variation as there was a clear positive excursion of $\delta^{13}C_{org}$ in the upper section sediments compared to the lower section of the P36 core profile with a minimum difference of 1.66‰ (Figure 3). Therefore, considering the finer sediment grain size distribution (Figures 2(b) and 2(c)) and the stable OM source, the higher content of TOC and TN in the upper

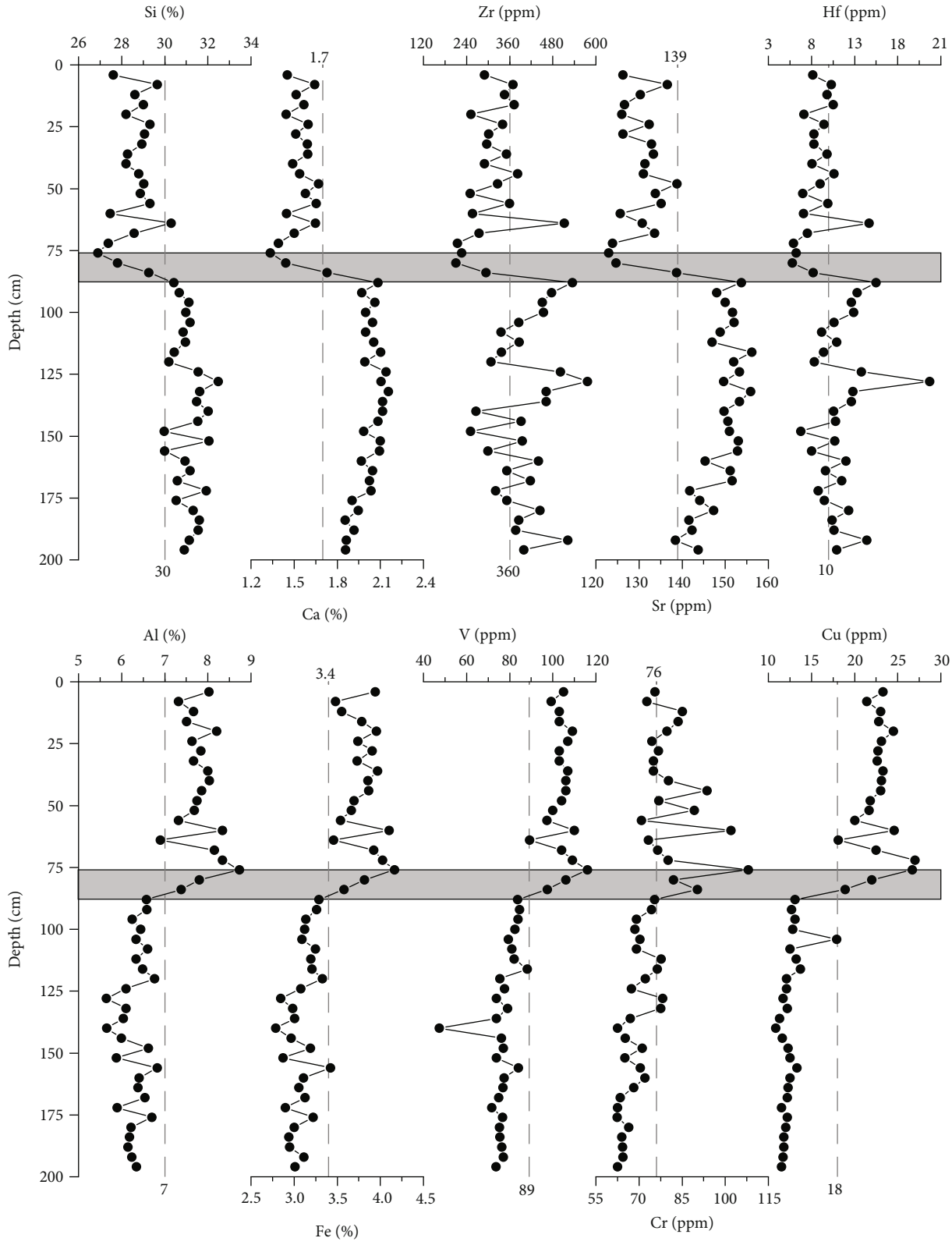

Figure 4: Profile variations of the average content of major and trace elements in P36 core during the Holocene. Note: the shaded region shows distinctly the transition of element content (76-90 cm) around the 3.2 kyr BP on the profile.

section was likely related to higher marine autogenous OM input and a better preservation condition for sedimentary OM due to the favorable marine environment.

Besides, the two-terminal mixed model with a single component tracer has been widely used to quantitatively estimate the contribution of terrestrial and marine OM for

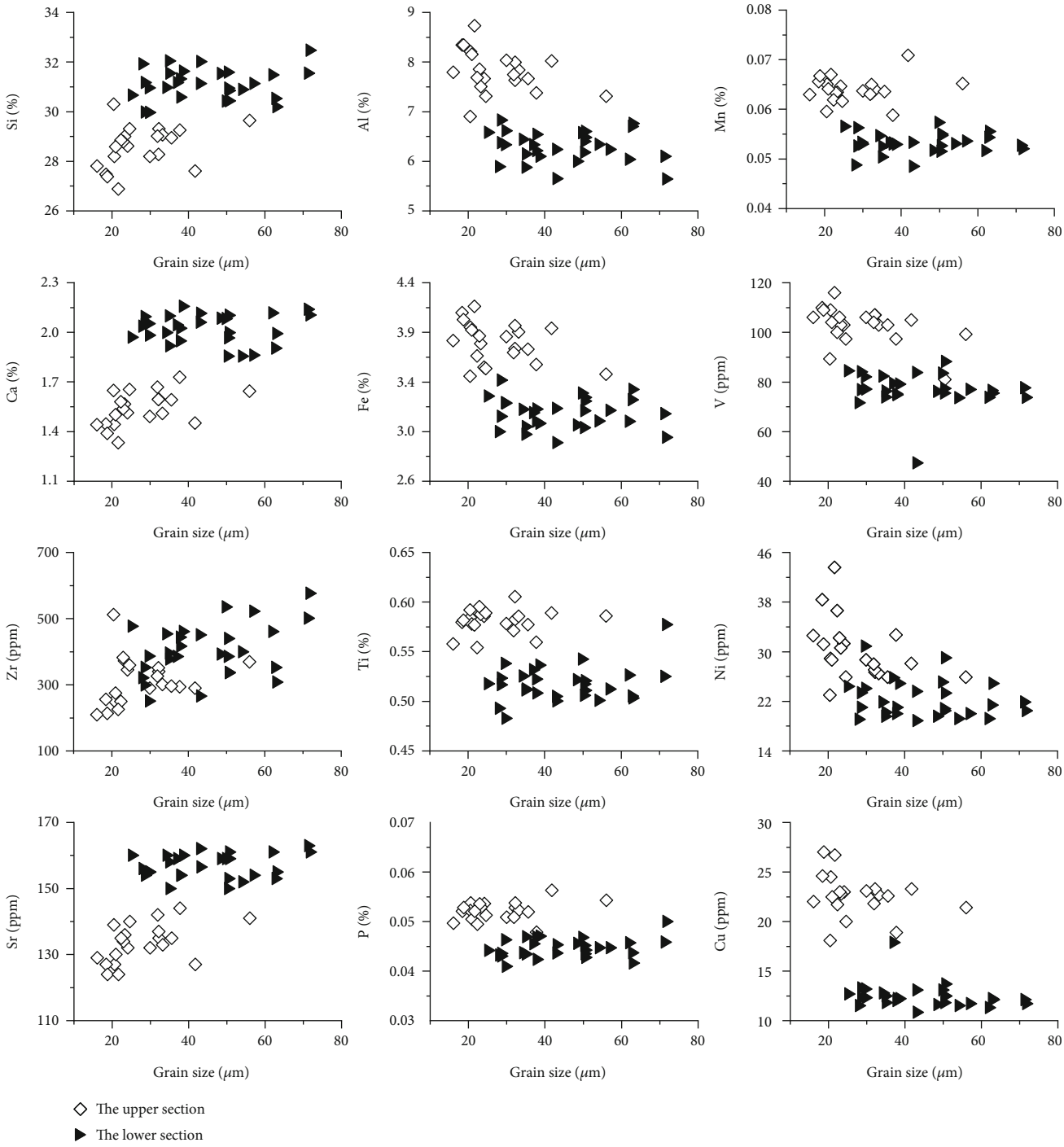

Figure 5: Plots of relationships between the element content and the mean grain size for the P36 core. Note: open rhombuses indicate sediments in the upper section of the P36 core; filled triangles represent sediments in the lower section of the P36 core.

marine sediments. The relative proportion and absolute content of marine authigenic organic carbon (OC_M) and terrestrial allochthonous organic carbon (OC_T) in sedimentary OM can be calculated through the binary model [61]. The specific calculation formula is as follows:

$$\delta^{13}C_{org} = f_M * \delta^{13}C_M + f_T * \delta^{13}C_T$$
$$f_M + f_T = 1 \quad (2)$$

In the marine system, the $\delta^{13}C_{org}$ composition of the phytoplankton is around -20‰ and is often considered as the carbon isotope composition of marine OM endmember ($\delta^{13}C_M$) [62]. It has been reported that the average of the $\delta^{13}C_M$ composition of OM of the Lingding Sea around the Pearl River Estuary is -20.5‰ [63, 64], and the $\delta^{13}C$ composition of particulate organic carbon in the Spring seawater from the nearby west mouth area of the Qiongzhou Strait is about -20.7‰ [65]; therefore, an average of -20.6‰ could

Table 2: Correlations between major elements, trace elements, Mz, REE, and organic matter in the sediments of P36 core (note: significant coefficients are given in bold; a total of 49 sample data were analyzed).

	SiO_2	Al_2O_3	Fe_2O_3	CaO	TiO_2	P_2O_5	MnO	LOI	CIA	V	Cr	Co	Ni	Cu	Zn	Rb	Sr	Ba	REE	Mz	Clay	TOC	TN	$\delta^{13}C$
SiO_2	1.00																							
Al_2O_3	-0.98	1.00																						
Fe_2O_3	-0.97	**0.99**	1.00																					
CaO	**0.91**	-0.94	-0.91	1.00																				
TiO_2	-0.73	0.78	**0.81**	-0.79	1.00																			
P_2O_5	-0.72	0.77	0.77	-0.83	**0.95**	1.00																		
MnO	-0.94	**0.96**	**0.96**	-0.92	**0.87**	**0.87**	1.00																	
LOI	-0.96	**0.93**	**0.91**	-0.90	0.68	0.71	**0.90**	1.00																
CIA	-0.83	**0.87**	**0.88**	-0.87	0.75	0.73	**0.83**	**0.81**	1.00															
V	-0.92	**0.95**	**0.95**	-0.89	**0.85**	**0.81**	**0.95**	**0.86**	**0.86**	1.00														
Cr	-0.73	0.73	0.74	-0.65	0.65	0.59	0.68	0.69	0.59	0.75	1.00													
Co	-0.95	**0.96**	**0.96**	-0.90	**0.81**	**0.80**	**0.95**	**0.90**	**0.86**	**0.97**	0.76	1.00												
Ni	-0.83	**0.81**	**0.81**	-0.72	0.62	0.59	0.75	0.77	0.66	**0.81**	**0.93**	**0.83**	1.00											
Cu	-0.92	**0.95**	**0.94**	-0.94	**0.88**	**0.88**	**0.95**	**0.87**	**0.87**	**0.94**	0.72	**0.95**	0.79	1.00										
Zn	-0.67	0.65	0.68	-0.54	0.56	0.50	0.65	0.60	0.54	0.69	0.67	0.67	0.79	0.64	1.00									
Rb	-0.42	0.46	0.47	-0.32	0.33	0.23	0.43	0.35	0.42	0.57	0.42	0.52	0.42	0.38	0.34	1.00								
Sr	0.91	-0.93	-0.91	**0.98**	-0.80	-0.84	-0.91	-0.91	-0.85	-0.87	-0.66	-0.90	-0.72	-0.94	-0.54	-0.30	1.00							
Ba	-0.40	0.38	0.38	-0.27	0.10	0.09	0.36	0.33	0.26	0.43	0.25	0.44	0.41	0.32	0.46	0.45	-0.21	1.00						
REE	0.06	-0.01	0.04	-0.07	0.47	0.40	0.15	-0.06	0.07	0.17	0.16	0.06	-0.03	0.08	0.03	0.17	-0.06	-0.27	1.00					
Mz	0.59	-0.60	-0.58	0.59	-0.43	-0.41	-0.51	-0.57	-0.57	-0.58	-0.49	-0.59	-0.57	-0.61	-0.46	-0.24	0.63	-0.23	0.17	1.00				
Clay	-0.80	**0.82**	**0.82**	-0.80	0.69	0.64	0.76	0.75	0.78	**0.80**	0.66	**0.80**	0.73	**0.83**	0.63	0.32	-0.81	0.29	-0.02	-0.91	1.00			
TOC	-0.91	**0.89**	**0.87**	-0.84	0.70	0.72	**0.90**	**0.87**	0.72	**0.84**	0.61	**0.88**	0.73	**0.86**	0.63	0.37	-0.87	0.34	-0.07	-0.58	0.75	1.00		
TN	-0.83	**0.81**	0.79	-0.76	0.64	0.66	**0.82**	**0.80**	0.69	0.74	0.53	0.76	0.65	0.77	0.61	0.19	-0.78	0.24	-0.06	-0.53	0.71	**0.87**	1.00	
$\delta^{13}C$	-0.86	**0.89**	**0.89**	-0.92	**0.88**	**0.89**	**0.92**	**0.85**	**0.83**	**0.90**	0.68	**0.89**	0.74	**0.95**	0.63	0.28	-0.91	0.18	0.16	-0.61	**0.82**	**0.84**	0.77	1.00

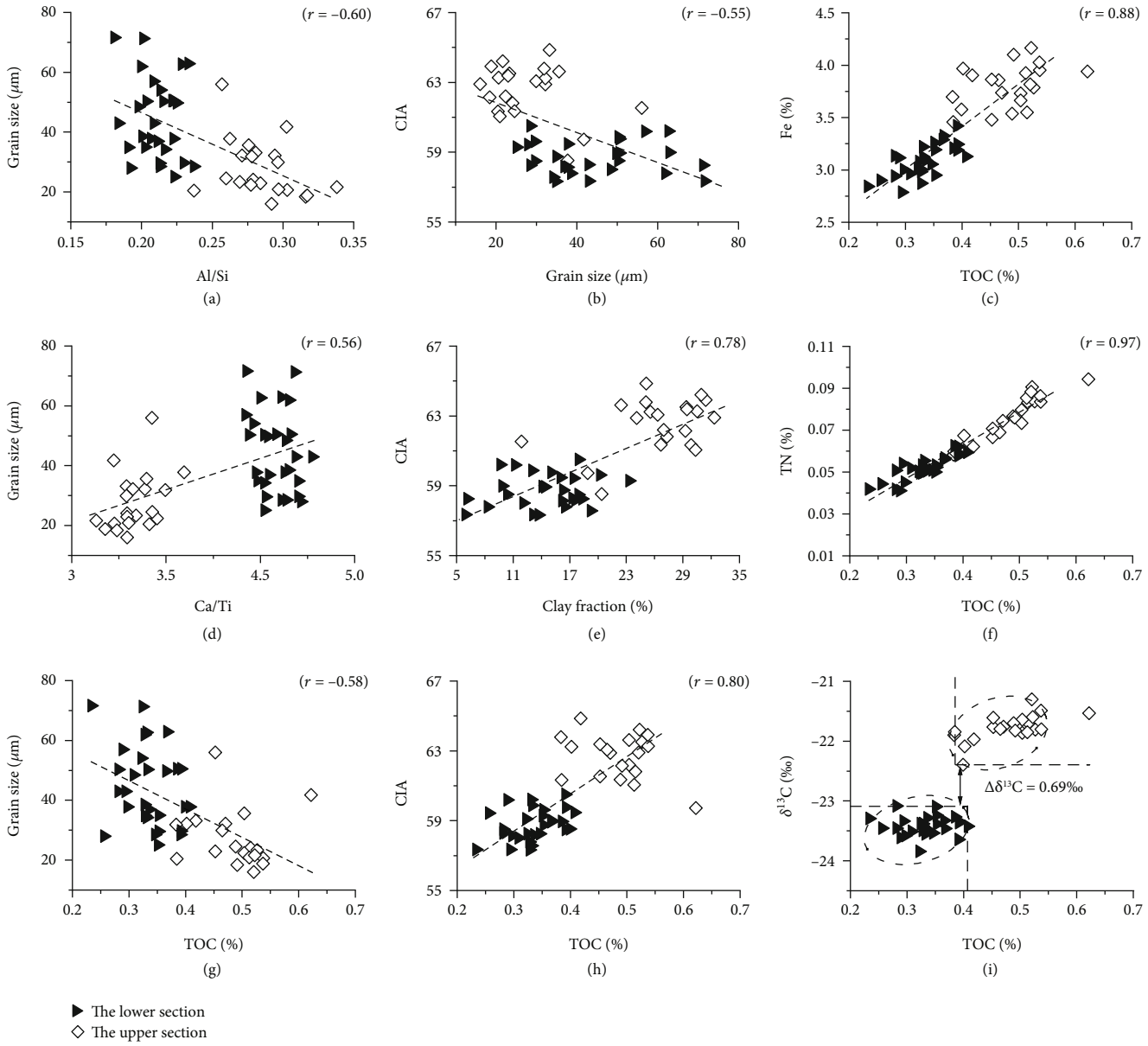

Figure 6: Relationships between grain size, clay fraction, CIA, and TOC with other key geochemical proxies of P36 core sediments. Note: open rhombuses indicate sediments in the upper section of the P36 core; filled triangles represent sediments in the lower section of the P36 core. Black dotted lines are best-fit regression lines, while *r* refers to correlation coefficient.

be used as the $\delta^{13}C_M$ composition in the northwest margin of the South China Sea including the Beibu Gulf. Considering that the average $\delta^{13}C$ composition of soil OM in the alluvial plain of the Pearl River is -24.1‰ [66], that the $\delta^{13}C$ composition of surface sediments in the Pearl River Estuary is -24.6‰ [64], and that the average $\delta^{13}C$ composition of suspended OM in the Nandu River of Hainan Island in the summer is -24.1‰ [67], an average $\delta^{13}C$ composition of -24.3‰ could be taken as the $\delta^{13}C_{org}$ composition of terrestrial OM endmember. And there, f_M and f_T are used to represent the proportion of marine and terrestrial organic carbon in the TOC.

Overall, the absolute content of OC_M of core sediments has gradually increased since the Holocene, reflecting the increase of marine authigenic OM. In the lower section, the f_M was less than 36% and the f_M was much smaller than the f_T, while the f_M was more than 73% in the upper section, indicating that the OM was mainly from the marine autogenous source after 3.2 kyr BP (Figure 3). As the estuarine intertidal zone with small runoff has the characteristics of low terrigenous OM contribution (3-35%) [68], the f_M of the P36 core during the late Holocene was likely to be affected by the input of small runoffs or lamellar flows from Hainan Island and the Leizhou Peninsula. The f_M in the P36 core dramatically increased from 31.3% to 86.8% (3.5 to 3.1 kyr BP) and then remained relatively stable at about 73% in the upper section sediments (Figure 3), suggesting that the terrigenous input during this period was probably

not the main reason causing the positive deviation of the $\delta^{13}C_{org}$ value in core sediments. So, the $\delta^{13}C_{org}$ composition of -21.29‰ to -22.09‰ for OM in the upper section sediments suggests that the OM in the upper section sediments was dominated by the marine autochthonous OM, while the $\delta^{13}C_{org}$ composition of -24.14‰ to -22.45‰ in the low section sediments may suggest that there was a higher proportion of terrigenous sourced organic matter inputs during the sedimentation of the lower section deposition (Figure 3).

Furthermore, as mentioned later, a positive correlation between the TOC content and the CIA ratio suggests that the increase of TOC content is consistent with a relatively stronger chemical weathering condition in the source region in that relatively warm and humid climate change might contribute to higher marine productivities (Figure 6(h)). The higher content of Fe in the upper section of the P36 core and the positive correlation of Fe content with the TOC content (Figures 4 and 6(c)) may also indicate that a large amount of Fe and other nutrient elements transported by rivers and aeolian dust from the surrounding mainland would lead to the enrichment of siderite in this sea area [69], promoting the increase of marine phytoplankton productivity [70], and thereby increasing the TOC content and the positive deviation of the $\delta^{13}C_{org}$ value in the P36 core (Figure 3). Therefore, the profile variations of TOC, TN, and the $\delta^{13}C_{org}$ composition all suggest that there was a significant change in the marine environment between the low section and upper section sediments.

4.3. The Profile Variation of Elemental Content and Their Environmental Implication. The dispersal and accumulation of elements in sediments are controlled by the sedimentary environment, the weather condition of source areas, and transportation distance and conditions, etc. [71]. The content of most of the major and trace elements and their ratios display a two-section distribution pattern in the P36 core as that of the grain size distribution (Figures 4, 5, 7). These suggest that the elemental compositions are generally controlled by the grain size. For a better understanding of the correlation among the elements with the sediment size, the correlation analysis was performed and illustrated in Figure 5 and Table 2. It can be seen that the variation of sediment grain size would lead to the difference in the content of most of the elements in P36 core sediments due to the effect of hydraulic sorting. Thus, the element ratio is used to weaken or eliminate the influence of sediment size sorting [72–74].

Among these elemental ratios, the Ti-normalized ratios can eliminate the effect of dilution by biogenic and authigenic element inputs on the content of elements in marine sediments [72]. The ratio of Si to Ti is likely to be a reflection of the changes in biogenic silica [75, 76] and can be used as an indicator to reflect the strength of the sedimentary hydrodynamic condition as a smaller ratio would suggest a weaker hydrodynamic condition [77, 78]. On the P36 profile, the Si/Ti ratio is in the range of 75 to 90 in the upper section sediments compared to the ratio range of 95 to 110 in the lower section sediments, and this distinctly proves a much weaker hydrodynamic condition during the deposition of the upper section sediments (Figure 7). Besides, the Ca/Ti ratio, which reflects the relative proportion of biogenic carbonate and terrigenous clastic, can be used as the proxy for clastic flux and terrigenous input [79–81]. Thus, the lower value of the Ca/Ti ratio in the upper section of the P36 core generally correlates with the intensified clastic delivery from the surrounding continent (Figure 7). Moreover, the higher value of the Al/Si ratio in the upper section of the P36 core also indicates that the content of clay fraction increases. And the relatively strong correlation of the Al/Si ratio with the grain size further indicates that the change of grain size was influenced by the input of terrigenous materials (Figure 6(a)).

The CIA index is also an important indicator that is often used to reflect the chemical weathering degree in the source area of sediments [48, 82, 83]. The CIA index of the P36 core sediments is in a range of 57 to 65, which indicates an incipient to intermediate chemical weathering condition under the relatively cold and dry climate conditions in the continental source area [84]. On the other hand, although the CIA index is in a narrow range on the whole profile, it also displays a two-section variation pattern as most of the CIA index was under 60 for the low section sediments but above 60 for the upper section sediments (Figure 7). Therefore, the relatively higher CIA index suggests that a slightly warm and humid weathering condition in the source region might have prevailed during the sedimentation period of the upper section, compared to the low section deposition period. Furthermore, since element Sr has a much higher geological activity than element Rb during weathering processes [85, 86], the relatively higher values of the Rb/Sr ratio in the upper section sediments also suggest a relatively intense chemical weathering during the upper section sedimentation (Figure 7).

In addition, some redox-sensitive trace elements (U, V, Cr, Co, Ni, Mo, etc.) in sediments are controlled by their variable behavior in response to different redox conditions, and their ratios, such as V/(V+Ni), U/Th, and Ni/Co, could be used to indicate the redox condition of the sedimentary environment during the sedimentation [87, 88]. Among these trace elements and their ratios, the U/Th, V/Cr, and Ni/Co ratios are distinctly less than 0.75, 2, and 5, respectively, and generally indicate an oxidizing environment [89]. However, the V/(V+Ni) ratio of P36 core sediments varies from 0.74 to 0.82 (Figure 7) suggesting a weakly stratified anoxic environment [90]. Because the V/(V+Ni) ratio usually infers a lower oxygen bottom-water condition (anoxic) than does either the Ni/Co or V/Cr ratios [91], and a higher content of V, Mo, Ni and Cu in the upper section sediments also indicates that there was a relatively reducing sedimentary environment which a higher OM flux brought these elements to the sediments [87]. Furthermore, the Cu/Zn ratio is also used to evaluate the paleoredox condition without the diagenesis influence [92, 93]. The lower average value of the Cu/Zn ratio (0.19) in the lower section sediments changes to a higher value (0.31) in the upper section sediments (Figure 7) indicating that the reduction environment transforms into the weak reduction environment. Therefore, the P36 core may deposit under the oxic to suboxic condition without significant sedimentary redox environmental change throughout the core profile.

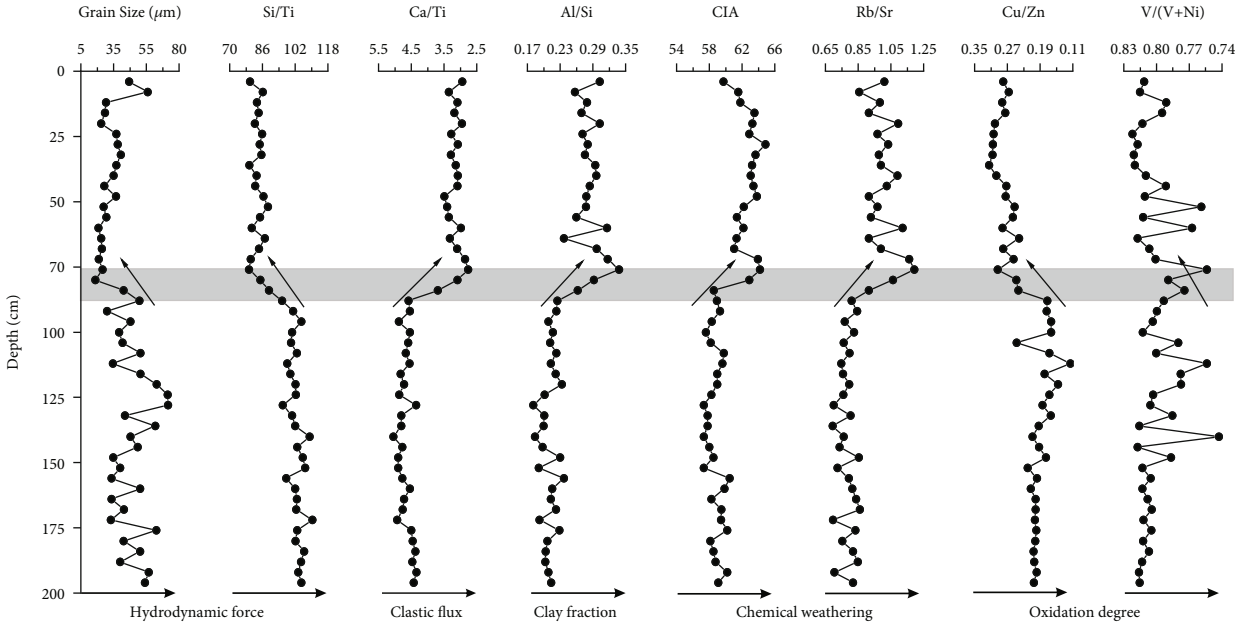

FIGURE 7: Profile variations in key element proxies used in this study show their response to the regional paleoclimate change and marine environment changes. The shaded region shows the distinct transition of the element ratio (76-90 cm) around the 3.2 kyr BP.

Since the location of the P36 core is near the western mouth of the Qiongzhou Strait, sediments in this area would have very complex source inputs that were derived from the erosion of earlier terrestrial sediments by the current inflowing through the Qiongzhou Strait developed since the Holocene [94], carried by the rivers surrounding the Beibu Gulf, such as the Pearl River and Red River, and come from the erosion of sediment from the nearby coastal region of the Leizhou Peninsula. Therefore, some extent of inconsistency among these redox-sensitive element proxies may be related to the complex source inputs of sediments, given that various sediment sources in this region along with the marine environmental change, especially the rise of the sea level in the Holocene around the Beibu Gulf, could affect the distribution of trace elements [91, 95, 96].

Under the same parent material source or similar sedimentary environment conditions, the geochemical parameters in sediments often show a certain correlation. Figure 6 shows a number of correlations among different geochemical components of core sediments. These correlations have a similar feature in that the core sediments are distributed in a continuous linear correlation but distinguished by two separated groups; i.e., the core sediments could be clearly grouped into the upper section and the lower section (Figure 6). And these continuous linear correlations undoubtedly indicate that sediment sources remain the same during the sedimentation of the upper and lower sections, but the sedimentary environment was likely changed. Obviously, the broad consistency in the profile distribution pattern of sediment grain size, CIA index, TOC content (Figure 6), and many other features clearly suggest that a dramatic shift occurred around 3.2 kyr BP in the marine environment between the upper and the lower section sedimentation, and this shift was likely related to the sea level change.

4.4. Marine Environment Change in the Beibu Gulf during the Holocene. As discussed above, it is clear that the low section sediments and upper section sediments were developed in different marine environment, as all geochemical features suggest that the upper section was developed under a deeper seawater condition, while the significant marine environment shift between the low and upper sections occurred around 3.2 kyr BP in the Beibu Gulf, and it is not clear whether this seawater depth change was due to the sea level rise or the seafloor subsidence.

The sea level fluctuation in the shallow continental shelf of the northern region of the South China Sea since the last deglaciation [18, 52, 97] could impose a significant influence on the marine environment of the Beibu Gulf during the Holocene. It has been reported that the abundance of the herb pollen and the microfossils of saltwater algae in the sediments of the eastern Beibu Gulf had drastically decreased and increased, respectively, from 13.4 to 11.4 kyr BP, which suggests that the Beibu Gulf had experienced a continuous transgression during the last deglaciation period [22]. As the transgression continued [13, 98], the sea level in the north margin of the South China Sea rose rapidly from about -48 m to -15 m at 11 to 9 kyr BP, and it rose slowly to the present sea level at 8 to 7 kyr BP [18, 52]. And the sea level might continue to rise a 1 to 3 m higher sea level than the present sea level during the Dong Da transgression period of 6 to 4 kyr BP [18, 97–101], and then, it may slowly drop to the present sea level after 4 to 3 kyr BP. Considering that the Beibu Gulf was basically terrestrial land during the last deglaciation period and the Qiongzhou Strait was

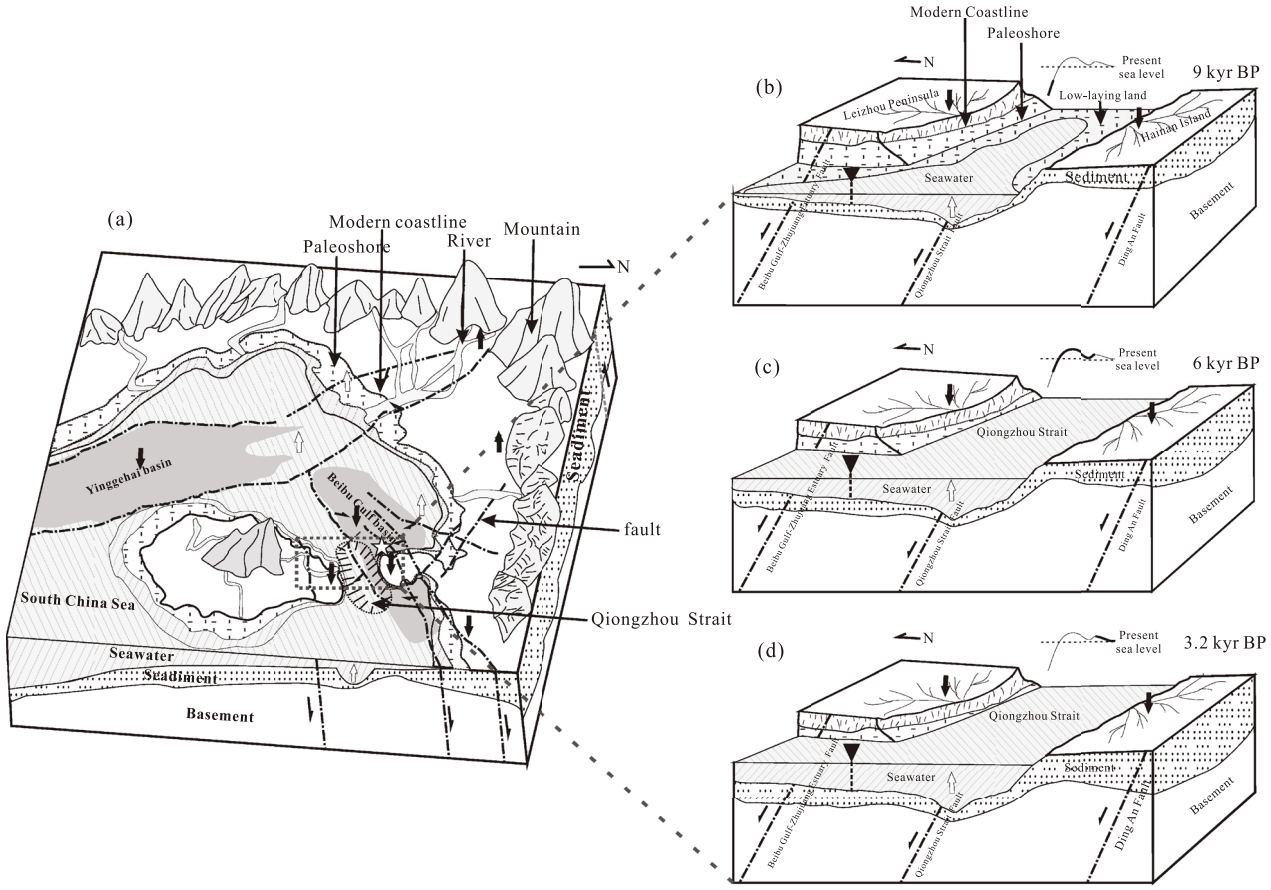

FIGURE 8: The conceptual graph of marine environmental change in the Beibu Gulf, showing the spatial variation of (a) the sea-level change and regional tectonic movement around the Beibu Gulf in the early-middle (11.3-3.2 kyr BP) and the late Holocene (3.2 kyr BP) indicated by the change of shoreline and (b–d) the sea-level change with the local subsidence in the sea area around the Qiongzhou strait during the Holocene. Note that the hollow asterisk and the black solid inverted triangle represent the location of the core P36.

eventually developed at about 11 to 7 kyr BP [22, 97, 102], it is expected that the sea level change in the north marginal sea of the South China sea could only have a limited effect on the change of the sedimentary environment of the northeastern Beibu Gulf after the 7 kyr BP.

As an underwater subsidence basin, the Beibu Gulf is passed through by the NW-SE-trending Red River fault zone in the central part of the Beibu Gulf, and long-term regional tectonic movements may cause its continual subsidence (Figure 8(a)). In addition, the P36 core was located around the LeiQiong depression zone that covers the south of the Leizhou Peninsula, Qiongzhou Strait, and the north of Hainan Island in the east of the Beibu Gulf [103–106], and the Qiongzhou Strait was formed by extensional faults caused by the differential crustal movement (Figure 8(a)) [105]. The local subsidence caused by fault activities in the LeiQiong depression zone would pull apart the Qiongzhou Strait that used to be the low-lying land during the last deglaciation and was gradually submerged by the sea during the Holocene (Figures 8(b)–8(d)). Since the channel of the Qiongzhou Strait progressively developed at about 10 kyr BP, the channel has been cut down from the original floodplain (-46.6 m) to a maximum depth of -73 m, with an annual average incised depth of about 0.7 cm [94].

As a result, when the sea level reached the present level in the late Holocene, land subsidence may have occurred in the southern part of the Leizhou Peninsula that once was the alluvial plain or the low-lying land [104] and finally led to the increase of seawater depth in the southwest offshore area of the Leizhou Peninsula (Figure 8). During this time, vertical accretion might also be the dominant deposition process in the Qiongzhou Strait caused by seabed downcut and deposit and strong monsoon-driven sediment discharge. The study of coral reef in the southwest sea area of the Leizhou Peninsula also indicates that the relative sea level was about 1.5 m higher than the present sea level at 3.2 kyr BP [107]. And the study of beach sediments and rocks around the coast of Beibu Gulf also shows that the sea level was still about 0.8 to 1.2 m higher than the present sea level until the late Holocene [108, 109], which probably confirmed the deepening of the seawater depth in the southwestern offshore area of the Leizhou Peninsula. Moreover, from 3.2 to 2.8 kyr BP, the sea level change in the Pearl River Delta was also on the rise with the relative sea level rising from about -1.0 m to 1.5 m [110]. As a result, this would inevitably result in the increase of seawater depth in the east coastal area of Guangdong. And since the Pearl River annually transports about 80 Mt of sediment to the South China

Sea, most of them are carried to the southwest shallow continental shelf area under the action of the Guangdong coastal current [111]. Under the influence of the NE-SW coastal current in the east of Guangdong, more sediments from the Pearl River and the Guangdong coastal area could also be carried by the coastal currents to the Beibu Gulf through the Qiongzhou Strait, especially since the 3.2 kyr BP when there was a significant marine environmental change in the Beibu Gulf, causing the significant increase in the sedimentation rate of the upper sections of the P36 core profile.

Thus, by referring to previous studies on the global sea level change [112, 113] and regional sea level variation in the north region of the South China Sea [18, 23, 97, 101], the marine environmental change in the Beibu Gulf reflected by the geochemical characteristics of P36 core sediments was due to the increase of seawater depth, while this seawater depth increase was most likely a combination of regional sea level rise and local seafloor subsidence in the Qiongzhou Strait and eastern Guangdong since the 3.2 kyr BP. However, it seems that the sea level might be dropped toward the present sea level at the late Holocene in the Beibu Gulf of the northwestern South China Sea, and the details may need more studies.

5. Conclusion

According to the profile variation of the sediment size, the content of major and trace elements, TOC, and TN, and the value of $\delta^{13}C_{org}$ on the P36 core sediments combined with AMS ^{14}C dating, the following points could be concluded:

(1) The P36 sediment core was mainly deposited during the Holocene period. And taking the buried depth of 86 cm as the boundary, the profile of the P36 core could be divided into two sedimentary sections based on the change of geochemical characteristics, i.e., the low section and the upper section. The upper section covers a depth range of 4 to 86 cm which represents the sedimentary records of 0.2 to 3.2 kyr BP, while the low section is in the depth range of 86 to 200 cm and represents the sedimentary records from 3.2 to 11.3 kyr BP

(2) In comparison to the lower section, the upper section is characterized by the higher content of TOC, TN, major elements (Al, Fe, Ti, Mn, and P), trace elements (such as Sc, V, Cr, Co, Ni, Cu, Zn, and Cs), and clay fraction minerals, but associated with the lower content of Si, Ca, Zr, Hf, and Sr and the sand fraction compared with the lower section. Furthermore, the $\delta^{13}C_{org}$ value of the upper section sediments is in the range of -21.29‰ to -22.09‰ which is heavier than the lower section sediments that ranged from -24.14‰ to -22.45‰ and shows a clear positive excursion. The 1.66‰ minimum positive deviation in the $\delta^{13}C_{org}$ value between the low and upper section sediments indicates a significant increase in the marine autogenous organic matter input during the upper section sedimentation

(3) All of these geochemical differences between the low and upper section sediments distinctly suggest that the low section was deposited under a relatively shallow seawater depth, while the upper section was developed under a deeper water depth condition. This dramatic marine environmental change between these two sections occurred around 3.2 kyr BP. Based on prior studies of the sea level change of the northern region of the South China Sea and tectonic movements in the Qiongzhou Strait during the Holocene, it is suggested that this dramatic marine environmental change was a combined result of regional sea level change and seafloor subsidence. Overall, our comprehensive review of paleoceanographic study from different sedimentary records shows how important multiproxy approaches can be to fully contribute to a better understanding of marine environmental change in the Beibu Gulf during the Holocene

Data Availability

The relevant data used to support the findings of this study is included within the article.

Conflicts of Interest

The authors declare that they have no known competing financial interests or personal relationships that could have appeared to influence the work reported in this paper.

Acknowledgments

This study is financially supported by the State Key Laboratory of Organic Geochemistry fund (SKLOG2020-2), the National Science Foundation of China (No. 41773037), and the Natural Science Foundation of Guangxi Province (No. 2018GXNSFBA050049). We are appreciative of Dr. Wang Xinyu and Dr. Cheng Zhineng of Guangzhou Institute of Geochemistry, Chinese Academy of Sciences, for their assistance in major elements and the AMS ^{14}C dating, respectively. And we are also grateful to Professor Zhang Zhengwei from the Institute of Geochemistry, Chinese Academy of Sciences, for the help with the measurement of trace elements.

References

[1] Q. Zhao and P. Wang, "Progress in quaternary paleoceanography of the South China Sea," *Quaternary Sciences*, vol. 6, pp. 3–5, 1999.

[2] L. J. Wang and P. X. Wang, "Late Quaternary paleoceanography of the South China Sea: glacial-interglacial contrasts in an enclosed basin," *Paleoceanography*, vol. 5, no. 1, pp. 77–90, 1990.

[3] J. Huang, F. Jiang, S. Wan, J. Zhang, A. Li, and T. Li, "Terrigenous supplies variability over the past 22,000 yr in the

southern South China Sea slope: relation to sea level and monsoon rainfall changes," *Journal of Asian Earth Sciences*, vol. 117, pp. 317–327, 2016.

[4] M. Li, T. Ouyang, C. Tian et al., "Sedimentary responses to the East Asian monsoon and sea level variations recorded in the northern South China Sea over the past 36 kyr," *Journal of Asian Earth Sciences*, vol. 171, pp. 213–224, 2019.

[5] J. G. Liu, R. Xiang, S. J. Kao, S. Y. Fu, and L. P. Zhou, "Sedimentary responses to sea-level rise and Kuroshio current intrusion since the Last Glacial Maximum: grain size and clay mineral evidence from the northern South China Sea slope," *Palaeogeography Palaeoclimatology Palaeoecology*, vol. 450, pp. 111–121, 2016.

[6] Z. F. Liu, Y. L. Zhao, C. Colin et al., "Source-to-sink transport processes of fluvial sediments in the South China Sea," *Earth-Science Reviews*, vol. 153, pp. 238–273, 2016.

[7] F. Liu, C. P. Yang, X. H. Chang, and Z. W. Liao, "Provenance discrimination of the last glacial sediments from the northeastern South China Sea and its paleoenvironmental indications," *Terrestrial Atmospheric and Oceanic Sciences*, vol. 29, no. 2, pp. 131–148, 2018.

[8] J. Huang, S. M. Wan, Z. F. Xiong et al., "Geochemical records of Taiwan-sourced sediments in the South China Sea linked to Holocene climate changes," *Palaeogeography Palaeoclimatology Palaeoecology*, vol. 441, no. 4, pp. 871–881, 2016.

[9] Q. Ge, J. P. Liu, Z. Xue, and F. Y. Chu, "Dispersal of the Zhujiang River (Pearl River) derived sediment in the Holocene," *Acta Oceanologica Sinica*, vol. 33, no. 8, pp. 1–9, 2014.

[10] Y. L. Liu, S. Gao, Y. P. Wang et al., "Distal mud deposits associated with the Pearl River over the northwestern continental shelf of the South China Sea," *Marine Geology*, vol. 347, pp. 43–57, 2014.

[11] D. K. Hu, P. D. Clift, P. Böning et al., "Holocene evolution in weathering and erosion patterns in the Pearl River Delta," *Geochemistry Geophysics Geosystems*, vol. 14, no. 7, pp. 2349–2368, 2013.

[12] M. S. Wu, Y. Q. Zong, K. M. Mok, K. M. Cheung, H. Xiong, and G. Huang, "Holocene hydrological and sea surface temperature changes in the northern coast of the South China Sea," *Journal of Asian Earth Sciences*, vol. 135, pp. 268–280, 2017.

[13] T. Liu and G. Li, "The spatial discrepancy of Holocene transgression in north Beibu Gulf of Guangxi coastline," *Haiyang Xuebao*, vol. 37, no. 3, pp. 70–76, 2015.

[14] Z. Cui, Z. Xia, J. Lin et al., *Holocene Environment Evolution and Anthropogenic Impact of Beibu Gulf, South China Sea*, China Ocean Press, Beijing, China, 2017.

[15] Y. Ni, R. Endler, Z. Xia et al., "The "butterfly delta" system of Qiongzhou Strait: morphology, seismic stratigraphy and sedimentation," *Marine Geology*, vol. 355, pp. 361–368, 2014.

[16] J. P. Zhang, M. Tomczak, A. Witkowski et al., "A diatom-based Holocene record of sedimentary and oceanographic environmental changes within the Beibu Gulf, NW South China Sea," *Marine Geology*, vol. 432, article 106395, 2021.

[17] Y. Ni, J. Harff, Z. Xia, J. J. Waniek, M. Endler, and D. E. Schulz-Bull, "Post-glacial mud depocentre in the southern Beibu Gulf: acoustic features and sedimentary environment evolution," *Geological Society, London, Special Publications*, vol. 429, no. 1, pp. 87–98, 2016.

[18] S. Tanabe, K. Hori, Y. Saito, S. Haruyama, V. P. Vu, and A. Kitamura, "Song Hong (Red River) delta evolution related to millennium-scale Holocene sea-level changes," *Quaternary Science Reviews*, vol. 22, no. 21-22, pp. 2345–2361, 2003.

[19] G. Li, Y. Bian, and P. Wang, "Holocene marine transgression and its micropaleontological characteristics in the northeastern waters of Beibu Gulf," *Tropic Oceanology*, vol. 7, no. 2, pp. 63–70, 1988.

[20] G. Li, W. Liang, S. Liao, and G. Fang, "Climatic changes since Holocene along Guangxi coast," *Marine Geology & Quaternary Geology*, vol. 16, no. 3, pp. 49–60, 1996.

[21] K. Hori, S. Tanabe, Y. Saito, S. Haruyama, V. Nguyen, and A. Kitamura, "Delta initiation and Holocene sea-level change: example from the Song Hong (Red River) delta, Vietnam," *Sedimentary Geology*, vol. 164, no. 3-4, pp. 237–249, 2004.

[22] Z. Li, Y. L. Zhang, Y. X. Li, and J. Zhao, "Palynological records of Holocene monsoon change from the Gulf of Tonkin (Beibuwan), northwestern South China Sea," *Quaternary Research*, vol. 74, no. 1, pp. 8–14, 2010.

[23] S. Tanabe, Y. Saito, Q. L. Vu, T. J. J. Hanebuth, Q. L. Ngo, and A. Kitamura, "Holocene evolution of the Song Hong (Red River) delta system, northern Vietnam," *Sedimentary Geology*, vol. 187, no. 1-2, pp. 29–61, 2006.

[24] K. F. Yu, J. X. Zhao, T. S. Liu, G. J. Wei, P. X. Wang, and K. D. Collerson, "High-frequency winter cooling and reef coral mortality during the Holocene climatic optimum," *Earth and Planetary Science Letters*, vol. 224, no. 1-2, pp. 143–155, 2004.

[25] K.-F. Yu, J.-X. Zhao, G.-J. Wei et al., "δ^{18}O, Sr/Ca and Mg/Ca records of Porites lutea corals from Leizhou Peninsula, northern South China Sea, and their applicability as paleoclimatic indicators," *Palaeogeography, Palaeoclimatology, Palaeoecology*, vol. 218, no. 1-2, pp. 57–73, 2005.

[26] K.-F. Yu, J.-X. Zhao, G.-J. Wei, X.-R. Cheng, and P.-X. Wang, "Mid-late Holocene monsoon climate retrieved from seasonal Sr/Ca and δ^{18}O records of Porites lutea corals at Leizhou Peninsula, northern coast of South China Sea," *Global and Planetary Change*, vol. 47, no. 2-4, pp. 301–316, 2005.

[27] H. Wanner, O. Solomina, M. Grosjean, S. P. Ritz, and M. Jetel, "Structure and origin of Holocene cold events," *Quaternary Science Reviews*, vol. 30, no. 21-22, pp. 3109–3123, 2011.

[28] P. A. Mayewski, E. E. Rohling, J. Curt Stager et al., "Holocene climate variability," *Quaternary Research*, vol. 62, no. 3, pp. 243–255, 2004.

[29] H. Renssen, H. Seppa, X. Crosta, H. Goosse, and D. M. Roche, "Global characterization of the Holocene thermal maximum," *Quaternary Science Reviews*, vol. 48, pp. 7–19, 2012.

[30] S. A. Marcott, J. D. Shakun, P. U. Clark, and A. C. Mix, "A reconstruction of regional and global temperature for the past 11,300 years," *Science*, vol. 339, no. 6124, pp. 1198–1201, 2013.

[31] G. Bond, W. Showers, M. Cheseby et al., "A pervasive millennial-scale cycle in North Atlantic Holocene and glacial climates," *Science*, vol. 278, no. 5341, pp. 1257–1266, 1997.

[32] G. Bond, B. Kromer, J. Beer et al., "Persistent solar influence on North Atlantic climate during the Holocene," *Science*, vol. 294, no. 5549, pp. 2130–2136, 2001.

[33] H. Wanner and J. Butikofer, "Holocene bond cycles: real or imaginary?," *Geografie*, vol. 113, no. 4, pp. 338–350, 2008.

[34] P. Breitenmoser, J. Beer, S. Brönnimann, D. Frank, F. Steinhilber, and H. Wanner, "Solar and volcanic fingerprints in tree-ring chronologies over the past 2000 years," *Palaeogeography, Palaeoclimatology, Palaeoecology*, vol. 313-314, pp. 127–139, 2012.

[35] D. M. Kong, G. J. Wei, M. T. Chen, S. Y. Peng, and Z. H. Liu, "Northern South China Sea SST changes over the last two millennia and possible linkage with solar irradiance," *Quaternary International*, vol. 459, pp. 29–34, 2017.

[36] M. E. Mann, Z. Zhang, S. Rutherford et al., "Global signatures and dynamical origins of the Little Ice Age and medieval climate anomaly," *Science*, vol. 326, no. 5957, pp. 1256–1260, 2009.

[37] G. T. Rustic, A. Koutavas, T. M. Marchitto, and B. K. Linsley, "Dynamical excitation of the tropical Pacific Ocean and ENSO variability by Little Ice Age cooling," *Science*, vol. 350, no. 6267, pp. 1537–1541, 2015.

[38] Z. Xia, J. J. Waniek, and T. Leipe, "Anthropogenic fingerprint in Beibu Gulf (South China Sea) sediments," *Journal of Coastal Research*, vol. 66, pp. 72–90, 2013.

[39] P. Xia, X. W. Meng, Z. Li, P. Zhi, M. Zhao, and E. Wang, "Late Holocene mangrove development and response to sea level change in the northwestern South China Sea," *Acta Oceanologica Sinica*, vol. 38, no. 11, pp. 111–120, 2019.

[40] M. C. Shi, C. S. Chen, Q. C. Xu et al., "The role of Qiongzhou Strait in the seasonal variation of the South China Sea circulation," *Journal of Physical Oceanography*, vol. 32, no. 1, pp. 103–121, 2002.

[41] D. X. Wu, Y. Wang, X. P. Lin, and J. Y. Yang, "On the mechanism of the cyclonic circulation in the Gulf of Tonkin in the summer," *Journal of Geophysical Research-Oceans*, vol. 113, no. C9, 2008.

[42] C. L. Chen, P. L. Li, M. C. Shi, J. Zuo, M. Chen, and H. Sun, "Numerical study of the tides and residual currents in the Qiongzhou Strait," *Chinese Journal of Oceanology and Limnology*, vol. 27, no. 4, pp. 931–942, 2009.

[43] M. Chen, X. Xie, W. Xiao, and D. Tan, "Yilan crater, a newly identified impact structure in Northeast China," *Chinese Science Bulletin*, vol. 65, no. 10, pp. 948–954, 2020.

[44] T. J. Heaton, P. Köhler, M. Butzin et al., "Marine20—the marine radiocarbon age calibration curve (0–55,000 cal BP)," *Radiocarbon*, vol. 62, no. 4, pp. 779–820, 2020.

[45] M. Stuiver and T. F. Braziunas, "Modeling Atmospheric14C influences and14C ages of marine samples to 10,000 BC," *Radiocarbon*, vol. 35, no. 1, pp. 137–189, 1993.

[46] Q. Hua, S. Ulm, K. Yu et al., "Temporal variability in the Holocene marine radiocarbon reservoir effect for the Tropical and South Pacific," *Quaternary Science Reviews*, vol. 249, article 106613, 2020.

[47] R. L. Folk, P. B. Andrews, and D. W. Lewis, "Detrital sedimentary rock classification and nomenclature for use in New Zealand," *New Zealand Journal of Geology and Geophysics*, vol. 13, no. 4, pp. 937–968, 1970.

[48] H. W. Nesbitt and G. M. Young, "Early proterozoic climates and plate motions inferred from major element chemistry of lutites," *Nature*, vol. 299, no. 5885, pp. 715–717, 1982.

[49] S. M. Mclennan, "Weathering and global denudation," *Journal of Geology*, vol. 101, no. 2, pp. 295–303, 1993.

[50] M. Blaauw and J. A. Christen, "Flexible paleoclimate age-depth models using an autoregressive gamma process," *Bayesian Analysis*, vol. 6, no. 3, pp. 457–474, 2011.

[51] K. Lambeck and J. Chappell, "Sea level change through the last glacial cycle," *Science*, vol. 292, no. 5517, pp. 679–686, 2001.

[52] Y. Q. Zong, K. Y. Huang, F. L. Yu et al., "The role of sea-level rise, monsoonal discharge and the palaeo-landscape in the early Holocene evolution of the Pearl River Delta, southern China," *Quaternary Science Reviews*, vol. 54, pp. 77–88, 2012.

[53] P. A. Meyers, "Preservation of elemental and isotopic source identification of sedimentary organic matter," *Chemical Geology*, vol. 114, no. 3-4, pp. 289–302, 1994.

[54] A. L. Lamb, G. P. Wilson, and M. J. Leng, "A review of coastal palaeoclimate and relative sea-level reconstructions using $\delta^{13}C$ and C/N ratios in organic material," *Earth-Science Reviews*, vol. 75, no. 1-4, pp. 29–57, 2006.

[55] S. F. Thornton and J. Mcmanus, "Application of organic carbon and nitrogen stable isotope and C/N ratios as source indicators of organic matter provenance in estuarine systems: evidence from the Tay Estuary, Scotland," *Estuarine Coastal and Shelf Science*, vol. 38, no. 3, pp. 219–233, 1994.

[56] J. D. Milliman, Q. C. Xie, and Z. S. Yang, "Transfer of particulate organic-carbon and nitrogen from the Yangtze-River to the ocean," *American Journal of Science*, vol. 284, no. 7, pp. 824–834, 1984.

[57] J. L. Xiao, J. W. Fan, D. Y. Zhai, R. L. Wen, and X. G. Qin, "Testing the model for linking grain-size component to lake level status of modern clastic lakes," *Quaternary International*, vol. 355, pp. 34–43, 2015.

[58] F. Li, H. Gao, L. Zhang, Z. Li, H. Pang, and B. Pan, "Grain size characteristics and evolution of core sedimentary environment in the Houtao plain reach of the Yellow River," *Acta Sedimentologica Sinica*, vol. 37, no. 6, pp. 1234–1243, 2019.

[59] J. W. Fan, H. C. Jiang, W. Shi et al., "A 450-year warming and wetting climate in southern Altay inferred from a Yileimu Lake sediment core," *Quaternary International*, vol. 592, pp. 37–50, 2021.

[60] L. Xing, H. L. Zhang, Z. N. Yuan, Y. Sun, and M. X. Zhao, "Terrestrial and marine biomarker estimates of organic matter sources and distributions in surface sediments from the East China Sea shelf," *Continental Shelf Research*, vol. 31, no. 10, pp. 1106–1115, 2011.

[61] D. J. Shultz and J. A. Calder, "Organic carbon $^{13}C^{12}C$ variations in estuarine sediments," *Geochimica et Cosmochimica Acta*, vol. 40, no. 4, pp. 381–385, 1976.

[62] A. Mackensen and G. Schmiedl, "Stable carbon isotopes in paleoceanography: atmosphere, oceans, and sediments," *Earth-Science Reviews*, vol. 197, article 102893, 2019.

[63] G. D. Jia and P. A. Peng, "Temporal and spatial variations in signatures of sedimented organic matter in Lingding Bay (Pearl estuary), southern China," *Marine Chemistry*, vol. 82, no. 1-2, pp. 47–54, 2003.

[64] J. F. Hu, P. A. Peng, G. D. Jia, B. X. Mai, and G. Zhang, "Distribution and sources of organic carbon, nitrogen and their isotopes in sediments of the subtropical Pearl River estuary and adjacent shelf, southern China," *Marine Chemistry*, vol. 98, no. 2-4, pp. 274–285, 2006.

[65] Y. He, F. Lin, M. Chen et al., "Carbon and nitrogen isotopic composition of particulate organic matter in the northern Beibu Gulf in spring," *Journal of Xiamen University (Natural Science)*, vol. 53, no. 2, pp. 246–251, 2014.

[66] F. Yu, Y. Zong, J. M. Lloyd et al., "Bulk organic $\delta^{13}C$ and C/N as indicators for sediment sources in the Pearl River delta and estuary, southern China," *Estuarine, Coastal and Shelf Science*, vol. 87, no. 4, pp. 618–630, 2010.

[67] U. K. Pradhan, *Sources and composition of organic carbon in tropical river systems: case studies from India and China, [Ph.D. thesis]*, East China Normal University, Shanghai, China, 2015.

[68] Y. S. Zhang, X. T. Xiao, D. Y. Liu et al., "Spatial and seasonal variations of organic carbon distributions in typical intertidal sediments of China," *Organic Geochemistry*, vol. 142, article 103993, 2020.

[69] D. Xu, *Sedimentary records since last deglaciation and the formation of modern sedimentary pattern in eastern Beibu Gulf, [Ph.D. thesis]*, Graduate School of Chinese Academy of Sciences (Institute of Oceanology), Qingdao, Shandong Province, China, 2014.

[70] A. O. Badejo, I. Seo, W. Kim, K. Hyeong, and S. J. Ju, "Effect of eolian Fe-supply change on the phytoplankton productivity and community in central equatorial Pacific Ocean during the Pleistocene: a lipid biomarker approach," *Organic Geochemistry*, vol. 112, pp. 170–176, 2017.

[71] G. M. Eskenazy, "Rare earth elements in a sampled coal from the Pirin deposit, Bulgaria," *International Journal of Coal Geology*, vol. 7, no. 3, pp. 301–314, 1987.

[72] G. J. Wei, Y. Liu, X. H. Li, L. Shao, and D. Y. Fang, "Major and trace element variations of the sediments at ODP site 1144, South China Sea, during the last 230 ka and their paleoclimate implications," *Palaeogeography Palaeoclimatology Palaeoecology*, vol. 212, no. 3-4, pp. 331–342, 2004.

[73] K. Kiminami and K. Fujii, "The relationship between major element concentration and grain size within sandstones from four turbidite sequences in Japan," *Sedimentary Geology*, vol. 195, no. 3-4, pp. 203–215, 2007.

[74] C. S. Zhang, L. J. Wang, G. S. Li, S. Dong, J. Yang, and X. Wang, "Grain size effect on multi-element concentrations in sediments from the intertidal flats of Bohai Bay, China," *Applied Geochemistry*, vol. 17, no. 1, pp. 59–68, 2002.

[75] N. L. Balascio, Z. H. Zhang, R. S. Bradley, B. Perren, S. O. Dahl, and J. Bakke, "A multi-proxy approach to assessing isolation basin stratigraphy from the Lofoten Islands, Norway," *Quaternary Research*, vol. 75, no. 1, pp. 288–300, 2011.

[76] W. C. Zhang, H. Yan, C. C. Liu et al., "Hydrological changes in Shuangchi Lake, Hainan Island, tropical China, during the Little Ice Age," *Quaternary International*, vol. 487, pp. 54–60, 2018.

[77] O. Dellwig, J. Hinrichs, A. Hild, and H. J. Brumsack, "Changing sedimentation in tidal flat sediments of the southern North Sea from the Holocene to the present: a geochemical approach," *Journal of Sea Research*, vol. 44, no. 3-4, pp. 195–208, 2000.

[78] C. Martin-Puertas, A. Brauer, P. Dulski, and B. Brademann, "Testing climate-proxy stationarity throughout the Holocene: an example from the varved sediments of Lake Meerfelder Maar (Germany)," *Quaternary Science Reviews*, vol. 58, pp. 56–65, 2012.

[79] P. D. Clift, S. Wan, and J. Blusztajn, "Reconstructing chemical weathering, physical erosion and monsoon intensity since 25 Ma in the northern South China Sea: a review of competing proxies," *Earth-Science Reviews*, vol. 130, pp. 86–102, 2014.

[80] S. Kaboth-Bahr, A. Bahr, K. A. Yamoah et al., "Rapid humidity changes across the Northern South China Sea during the last ~40 kyrs," *Marine Geology*, vol. 440, article 106579, 2021.

[81] Y. B. Sun, J. F. McManus, S. C. Clemens et al., "Persistent orbital influence on millennial climate variability through the Pleistocene," *Nature Geoscience*, vol. 14, no. 11, pp. 812–818, 2021.

[82] G. Wei, X. H. Li, Y. Liu, L. Shao, and X. R. Liang, "Geochemical record of chemical weathering and monsoon climate change since the early Miocene in the South China Sea," *Paleoceanography*, vol. 21, no. 4, 2006.

[83] P. D. Clift, D. K. Kulhanek, P. Zhou et al., "Chemical weathering and erosion responses to changing monsoon climate in the late Miocene of Southwest Asia," *Geological Magazine*, vol. 157, no. 6, pp. 939–955, 2020.

[84] C. M. Fedo, H. W. Nesbitt, and G. M. Young, "Unraveling the effects of potassium metasomatism in sedimentary-rocks and paleosols, with implications for paleoweathering conditions and provenance," *Geology*, vol. 23, no. 10, pp. 921–924, 1995.

[85] E. J. Dasch, "Strontium isotopes in weathering profiles, deep-sea sediments, and sedimentary rocks," *Geochimica et Cosmochimica Acta*, vol. 33, no. 12, pp. 1521–1552, 1969.

[86] Z. D. Jin, J. J. Cao, J. L. Wu, and S. M. Wang, "A Rb/Sr record of catchment weathering response to Holocene climate change in Inner Mongolia," *Earth Surface Processes and Landforms*, vol. 31, no. 3, pp. 285–291, 2006.

[87] N. Tribovillard, T. J. Algeo, T. Lyons, and A. Riboulleau, "Trace metals as paleoredox and paleoproductivity proxies: an update," *Chemical Geology*, vol. 232, no. 1-2, pp. 12–32, 2006.

[88] T. J. Algeo and J. B. Maynard, "Trace-element behavior and redox facies in core shales of upper Pennsylvanian Kansas-type cyclothems," *Chemical Geology*, vol. 206, no. 3-4, pp. 289–318, 2004.

[89] B. Jones and D. A. C. Manning, "Comparison of geochemical indices used for the interpretation of palaeoredox conditions in ancient mudstones," *Chemical Geology*, vol. 111, no. 1-4, pp. 111–129, 1994.

[90] J. R. Hatch and J. S. Leventhal, "Relationship between inferred redox potential of the depositional environment and geochemistry of the Upper Pennsylvanian (Missourian) Stark Shale Member of the Dennis Limestone, Wabaunsee County, Kansas, USA," *Chemical Geology*, vol. 99, no. 1-3, pp. 65–82, 1992.

[91] S. M. Rimmer, "Geochemical paleoredox indicators in Devonian-Mississippian black shales, Central Appalachian Basin (USA)," *Chemical Geology*, vol. 206, no. 3-4, pp. 373–391, 2004.

[92] H. Dypvik, "Geochemical compositions and depositional conditions of upper Jurassic and lower Cretaceous Yorkshire clays, England," *Geological Magazine*, vol. 121, no. 5, pp. 489–504, 1984.

[93] R. O. Hallberg, "A geochemical method for investigation of palaeoredox conditions in sediments," *Ambio Special Report*, vol. 4, no. 4, pp. 139–147, 1976.

[94] H. Zhao, L. Wang, and J. Yuan, "Origin and time of Qiongzhou Strait," *Marine Geology and Quaternary Geology*, vol. 27, no. 2, pp. 33–40, 2007.

[95] S. S. Acharya, M. K. Panigrahi, A. K. Gupta, and S. Tripathy, "Response of trace metal redox proxies in continental shelf

environment: the eastern Arabian Sea scenario," *Continental Shelf Research*, vol. 106, pp. 70–84, 2015.

[96] J. L. McKay, T. F. Pedersen, and A. Mucci, "Sedimentary redox conditions in continental margin sediments (N.E. Pacific) – influence on the accumulation of redox-sensitive trace metals," *Chemical Geology*, vol. 238, no. 3-4, pp. 180–196, 2007.

[97] Y. T. Yao, J. Harff, M. Meyer, and W. H. Zhan, "Reconstruction of paleocoastlines for the northwestern South China Sea since the Last Glacial Maximum," *Science in China Series D-Earth Sciences*, vol. 52, no. 8, pp. 1127–1136, 2009.

[98] A. M. Korotky, N. G. Razjigaeva, L. A. Ganzey et al., "Late Pleistocene-Holocene coastal development of islands off Vietnam," *Journal of Southeast Asian Earth Sciences*, vol. 11, no. 4, pp. 301–308, 1995.

[99] B. Nie, "Sea-level changes of the South China Sea in the past 5000 years," *Quartenary Sciences*, vol. 1, pp. 80–87, 1996.

[100] X. Li, J. Han, R. Tang et al., "Holocene palaeoclimatic changes in the northern South China Sea," *Geological Research of South China Sea*, vol. 9, pp. 86–104, 1997.

[101] Z. Yongqiang, "Mid-Holocene sea-level highstand along the southeast coast of China," *Quaternary International*, vol. 117, no. 1, pp. 55–67, 2004.

[102] Y. Ni, Z. Xia, and S. Ma, "The opening of Qiongzhou Strait: evidence from sub-bottom profiles," *Marine Geology & Quaternary Geology*, vol. 34, no. 4, pp. 79–82, 2014.

[103] H. Zhang and X. Zhao, "Characteristics of the neotectonic movement in the Hainan Island and Leizhou Peninsula area," *Chinese Journal of Geology*, vol. 19, no. 3, pp. 276–287, 1984.

[104] H. Zhang and W. Chen, "A search for the cause of Qiongzhou Strait," *Acta Oceanologica Sinica*, vol. 9, no. 5, pp. 594–602, 1987.

[105] X. Lin and Y. Zong, "More on the origin of the Qiongzhou Strait," *Tropical Geography*, vol. 7, no. 4, pp. 338–345, 1987.

[106] B. Jin, C. Bao, and J. Lin, "Geomorphic feature and origin of the deltas at the east and west mouthes of Qiongzhou Strait," *Marine Geological Research*, vol. 2, no. 4, pp. 94–101, 1982.

[107] K. F. Yu, "Coral reefs in the South China Sea: their response to and records on past environmental changes," *Science China-Earth Sciences*, vol. 55, no. 8, pp. 1217–1229, 2012.

[108] K. Yu and T. Chen, "Beach sediments from northern South China Sea suggest high and oscillating sea levels during the late Holocene," *Earth Science Frontiers*, vol. 16, no. 6, pp. 138–145, 2009.

[109] W. Liu, K. Yu, R. Wang, and T. Yan, "Uranium-series ages of Beigang beach rock at Weuzhou Island and their significance in recordings sea level variations," *Quaternary Sciences*, vol. 40, no. 3, pp. 764–774, 2020.

[110] P. Li, P. Qiao, H. Zheng, G. Fang, and G. Huang, *The Environment Evolution of the Zhujiang Delta in the Last 10000 Years*, China Ocean Press, Beijing, China, 1991.

[111] Y. Zhong, Z. Chen, L. Li et al., "Bottom water hydrodynamic provinces and transport patterns of the northern South China Sea: evidence from grain size of the terrigenous sediments," *Continental Shelf Research*, vol. 140, pp. 11–26, 2017.

[112] T. M. Cronin, "Rapid sea-level rise," *Quaternary Science Reviews*, vol. 56, pp. 11–30, 2012.

[113] W. R. Gehrels, B. P. Horton, A. C. Kemp, and D. Sivan, "Two millennia of sea level data: the key to predicting change," *Eos, Transactions American Geophysical Union*, vol. 92, no. 35, pp. 289-290, 2011.